Titolo

ANALYSIS OF ANOMALOUS MEASUREMENTS OF RADIONUCLIDES IN NORTHERN AND EASTERN EUROPE IN JUNE 2020

Descrittori

Tipologia del documento: Rapporto tecnico

Collocazione contrattuale:

Argomenti trattati: Radioactivity measurements, reactor burn-up calculations, atmospheric dispersion, emergency preparedness and response

Sommario

Questo rapporto riporta le analisi effettuate su una serie di misure radiologiche anomale di isotopi prodotti da fissione nucleare registrate nel nord ed est Europa durante il mese di Giugno 2020.
Diverse metodologie vengono esplorate per determinare la possibile sorgente di emissione di questi elementi radioattivi: analisi dei rapporti isotopici in correlazione alla quantità di isotopi presenti nel combustibile esausto e simulazioni di traiettorie e dispersione di inquinanti radioattivi in atmosfera.
I risultati ottenuti vengono poi analizzati nell'insieme per dedurre i possibili scenari di rilascio.
Questo rapporto è redatto in lingua inglese.

Autori

Antonio Cervone, Antonio Guglielmelli

Note

Revisione 1: modifica ai ringraziamenti.

Copia n. **In carico a:**

REV.	DESCRIZIONE	DATA		REDAZIONE	CONVALIDA	APPROVAZIONE
2			NOME			
			FIRMA			
1	REVISIONE	30/07/20	NOME	A. CERVONE	F. ROCCHI	P. MELONI
			FIRMA	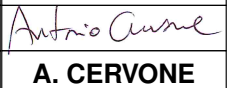	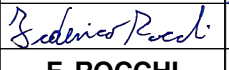	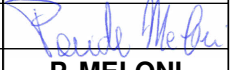
0	EMISSIONE	29/07/20	NOME	A. CERVONE	F. ROCCHI	P. MELONI
			FIRMA			

Analysis of anomalous measurements of radionuclides in Northern and Eastern Europe in June 2020

A. Cervone, A. Guglielmelli
ENEA FSN/SICNUC/SIN

Wednesday 29th July, 2020

Contents

1 Anomalous measurements

During the month of June 2020 several anomalous measurements of radioactive nuclides have been recorded in different countries in Scandinavia and Eastern Europe. The measurements reported are considered anomalous because they consist of a mixture of several artificial radionuclides, comprising neutron activation products as well as long and short-lived fission products, which are not found in the natural background, including the fallout of the Chernobyl 1986 accident, with the notable exception of Cs-137. The aim of this report is to analyze the available data in order to advance plausible hypotheses on the nature of the radionuclide source and origin.

The laboratories that registered those measurements are part of two major partnerships in radioactive measurements in the atmosphere, namely

- the *Ring of 5*, a European network of radioactivity experts, that includes several laboratories in most European countries;
- the *Comprehensive Nuclear-Test-Ban Treaty Organization (CTBTO)*, the international organization in charge of the verification of the ban on nuclear explosion tests, that includes, among other, a worldwide network of radionuclide measurement stations.

Following the publication of the CTBTO measurements, the Incident and Emergency Center (IEC) of IAEA started to collect and publish all the relevant measured data. All the measurements used in this report are taken from the public IAEA reports[1, 2].

The location of the laboratories that provided the measurements that will be discussed in this report are shown in Figure 1.1.

1.1 Ring Of 5 Laboratories

The first laboratory that provided some measurements that were outside the normal concentrations was Helsinki (Finland), around June 23rd. Their measurements are reported

Table 1.1: Helsinki anomalous measurements.

isotope	value [uBq/m3]	uncertainty (%)	start date	end date
Co-60	7.6	13.0	2020-06-16 08:00	2020-06-17 08:00
Ru-103	5.1	18.0	2020-06-16 08:00	2020-06-17 08:00
Cs-134	22.0	5.0	2020-06-16 08:00	2020-06-17 08:00
Cs-137	16.9	9.0	2020-06-16 08:00	2020-06-17 08:00

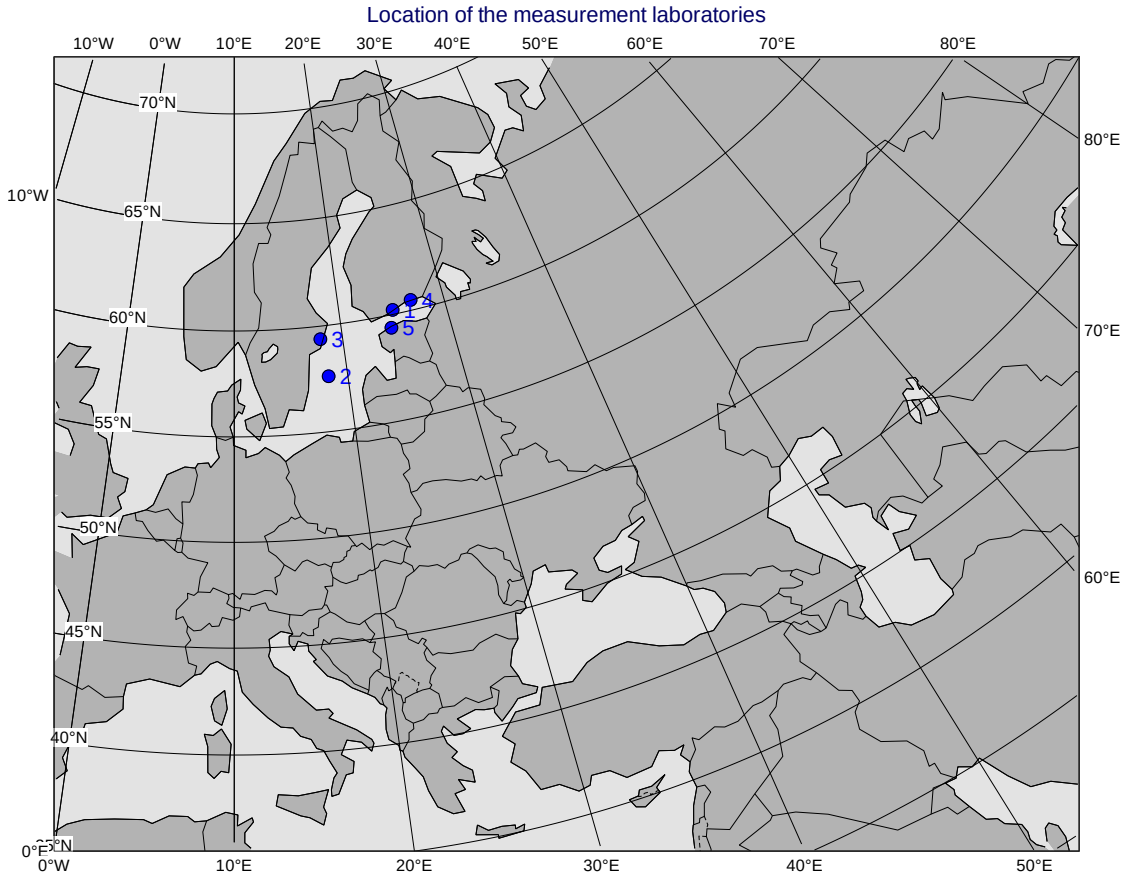

id	place	source	latitude	longitude
1	Helsinki	Ro5	60.21	25.05
2	Visby	Ro5	57.61	18.32
3	Stockholm/RN63	CTBTO	59.39	17.96
4	Kotka	Ro5	60.48	26.92
5	Harku	Ro5	59.40	24.60

Figure 1.1: Location of the laboratories which registered anomalous measurements.

Table 1.2: Visby anomalous measurements.

isotope	value [uBq/m3]	uncertainty (%)	start date	end date
Cs-134	0.77	5.0	2020-06-08 08:00	2020-06-15 08:00
Cs-137	1.34	6.0	2020-06-08 08:00	2020-06-15 08:00
Ru-103	0.10	42.0	2020-06-08 08:00	2020-06-15 08:00
Co-60	0.22	23.0	2020-06-08 08:00	2020-06-15 08:00
Cs-134	0.61	7.0	2020-06-15 08:00	2020-06-22 08:00
Cs-137	0.69	10.0	2020-06-15 08:00	2020-06-22 08:00
Ru-103	0.71	10.0	2020-06-15 08:00	2020-06-22 08:00
Ru-106	1.44	49.0	2020-06-15 08:00	2020-06-22 08:00
Nb-95	0.99	6.0	2020-06-15 08:00	2020-06-22 08:00
Zr-95	0.69	9.0	2020-06-15 08:00	2020-06-22 08:00
Co-60	0.39	18.0	2020-06-15 08:00	2020-06-22 08:00

Table 1.3: Kotka anomalous measurements.

isotope	value [uBq/m3]	uncertainty (%)	start date	end date
Co-60	0.7	5.0	2020-06-15 00:00	2020-06-22 00:00
Zr-95	0.2	20.0	2020-06-15 00:00	2020-06-22 00:00
Nb-95	0.4	10.0	2020-06-15 00:00	2020-06-22 00:00
Ru-103	0.3	10.0	2020-06-15 00:00	2020-06-22 00:00
Cs-134	1.7	4.0	2020-06-15 00:00	2020-06-22 00:00
Cs-137	2.4	5.0	2020-06-15 00:00	2020-06-22 00:00
Ce-141	0.2	18.0	2020-06-15 00:00	2020-06-22 00:00

in Table 1.1.

Soon after the alert from Helsinki, other measurements were provided by the Visby (Sweden) laboratory for the week between June 8th and June 15th. Their measurements can be seen in Table 1.2, together with the measurements for the week between June 15th and June 22nd.

Another laboratory in Finland, located in Kotka, confirmed the measurements from Helsinki in the same period. These measurements are reported in Table 1.3.

Finally, other measurements of the same nuclides were also registered by the laboratory in Harku (Estonia). These final measurements from the Ring of 5 are reported in Table 1.4.

1.2 CTBTO Stations

In the week following the alert from the Ring of 5 laboratories, new anomalous measurements of the same nuclides were registered by the CTBTO Radionuclides Station in

Table 1.4: Harku anomalous measurements.

isotope	value [uBq/m3]	uncertainty (%)	start date	end date
Cs-134	2.80	4.0	2020-06-14 00:00	2020-06-21 00:00
Cs-137	2.50	6.0	2020-06-14 00:00	2020-06-21 00:00
Ru-103	0.28	2.8	2020-06-14 00:00	2020-06-21 00:00
Co-60	0.69	16.0	2020-06-14 00:00	2020-06-21 00:00

Table 1.5: Stockholm anomalous measurements.

isotope	value [uBq/m3]	uncertainty (%)	start date	end date
Na-24	19.70	31.69	2020-05-31 09:00	2020-06-01 09:00
Cs-137	2.47	27.16	2020-06-10 09:00	2020-06-11 09:00
Cs-137	2.10	33.81	2020-06-11 09:00	2020-06-12 09:00
Cs-134	9.66	10.04	2020-06-22 09:00	2020-06-23 09:00
Cs-137	9.55	9.21	2020-06-22 09:00	2020-06-23 09:00
Ru-103	4.30	18.02	2020-06-22 09:00	2020-06-23 09:00
Na-24	20.30	35.33	2020-06-24 09:00	2020-06-25 09:00

Stockholm (Sweden), designed as RN63. These measurements are reported in Table 1.5.

1.3 Temporal correlation among different stations

Table 1.6 reports all the relevant isotopes half-lives for easiness of comprehension of the following sections, together with their production mechanisms and MELCOR chemical class[3], that puts together elements that behave similarly, have similar release fraction and follow the same path in case of an incident in a NPP.

In order to correlate all these measurements it is important to assess their relative

Table 1.6: Relevant isotopes characteristics.

Isotope	Half-life	Origin	MELCOR chemical class
Ru-103	39.26 d	Fission/Activation	6 - Platinoids
Ru-106	373.6 d	Fission	6 - Platinoids
Cs-134	2.06 y	Fission/Activation	2 - Alkali Metals
Cs-137	30.17 y	Fission/Activation	2 - Alkali Metals
Zr-95	65 d	Fission/Activation	8 - Tetravalents
Ce-141	32.5 d	Fission/Activation	8 - Tetravalents
Co-60	5.3 y	Activation	7 - Transition Metals
Nb-95	35 d	Fission/Activation	7 - Transition Metals

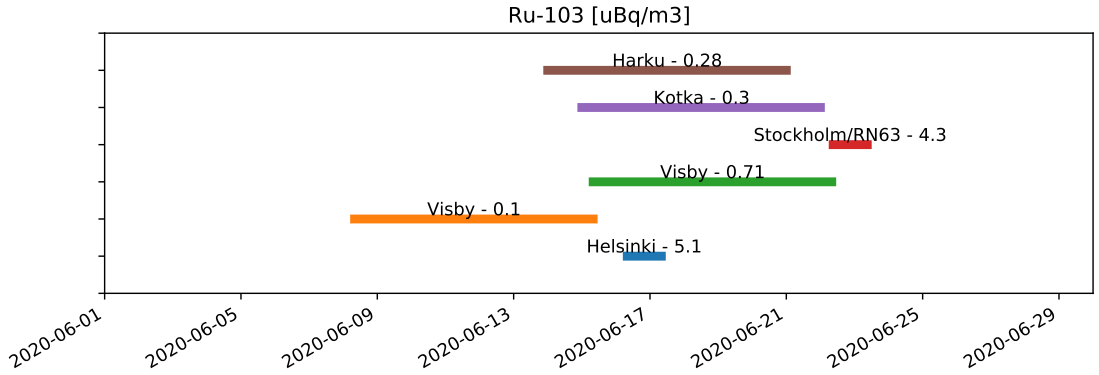

Figure 1.2: Distribution of Ru-103 measurements in the month of June 2020.

position in time. In fact, measurements of the same isotope happening in different locations at different times can or cannot have a common source, based on atmospheric recirculation patterns.

Some limitations of the computational tools in the backward simulation of the dispersion of such radionuclides in the atmosphere are a key factor in the ability to properly pinpoint a source (and a time duration) that correlates appropriately to all the measurements. In particular, in the backward motion of a pollutant in the atmosphere, the motion component dictated by the mean wind is inverted by inverting the time step but, on the other hand, the turbulent stochastic component of the motion is still computed in the same way as in the forward simulations. The consequence of this methodology is that, the more the simulation goes back in time, the more the source-receptor-sensitivity (SRS) matrix is spread over a wider area.

This means that backward simulations starting from points far away in time (a few days or more, depending on the instability of the atmosphere in the selected period) lead to poor combined sensitivities, as we will see in the following, and therefore a scarce capacity to pinpoint specific locations.

It must be highlighted also that, for this particular case, the location of all the measurement sites is concentrated in a small region of space that is subject to common recirculation pattern in the atmosphere. This is an additional cause of degraded performance of the backward simulation comparison, since the closer the locations, the higher the probability that the SRS maps will follow a similar pattern in the backward motion.

Figures 1.2–1.9 report synoptically all the measurements from the previous tables divided by isotope and displayed on a time axis in order to assess the extension and closeness in time of the measures in different locations.

In particular, we can see in Figure 1.2 that the measures of Ru-103 are spread across more than two weeks, and that only the Helsinki and Stockholm measures were made over a single day, all the others use a whole week collection period. Comparatively, and rather surprisingly, there is only a single Ru-106 measure (in Figure 1.3). This strange absence (Ru-103 and Ru-106 are in fact both simultaneously and abundantly produced

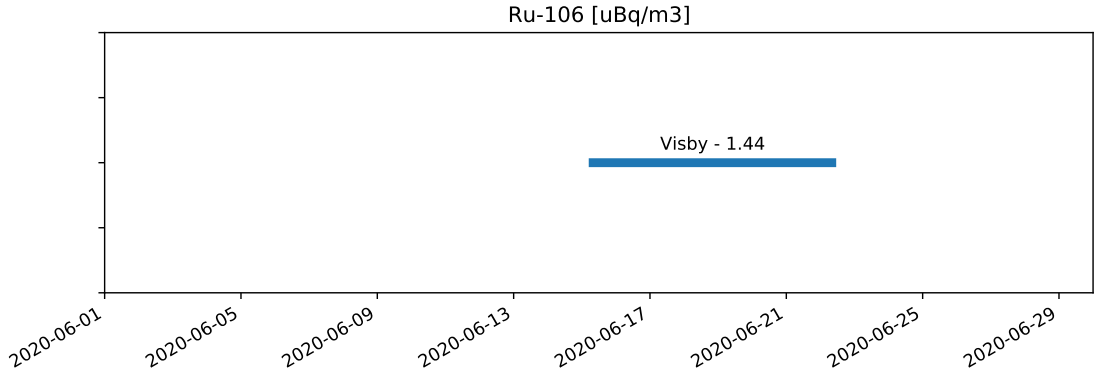

Figure 1.3: Distribution of Ru-106 measurements in the month of June 2020.

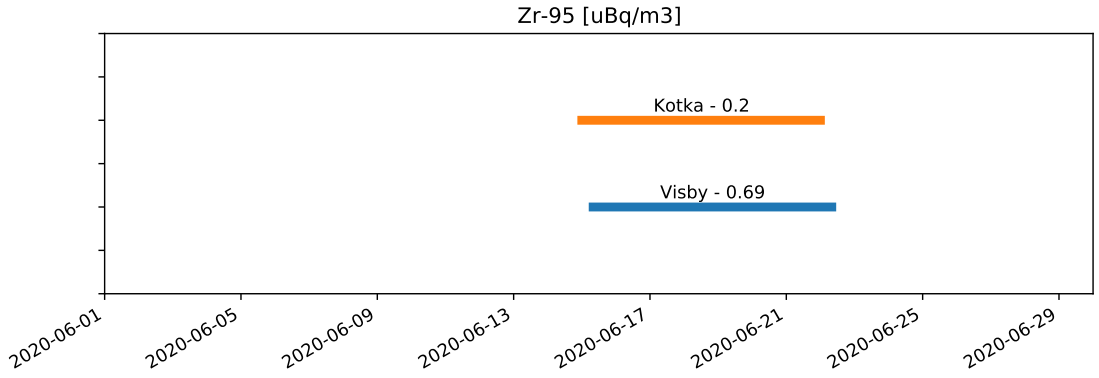

Figure 1.4: Distribution of Zr-95 measurements in the month of June 2020.

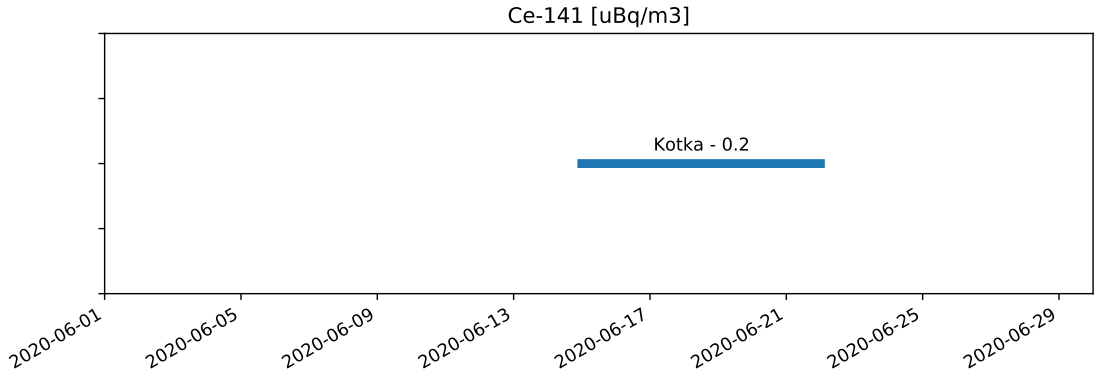

Figure 1.5: Distribution of Ce-141 measurements in the month of June 2020.

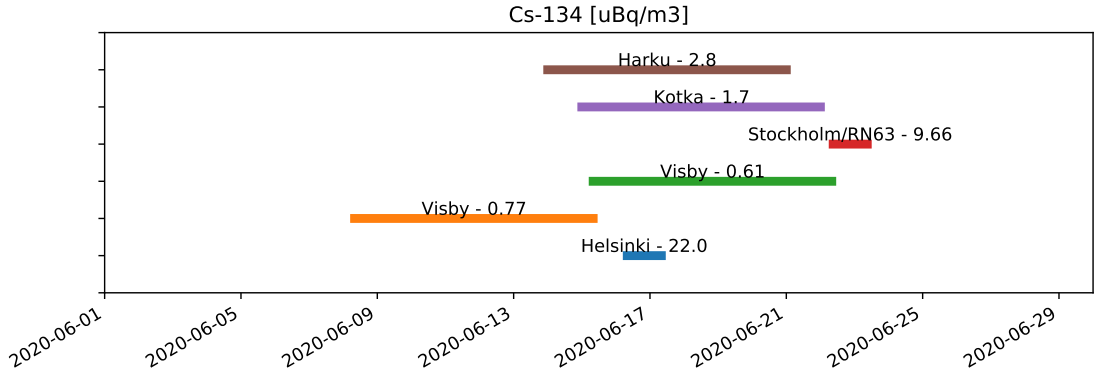

Figure 1.6: Distribution of Cs-134 measurements in the month of June 2020.

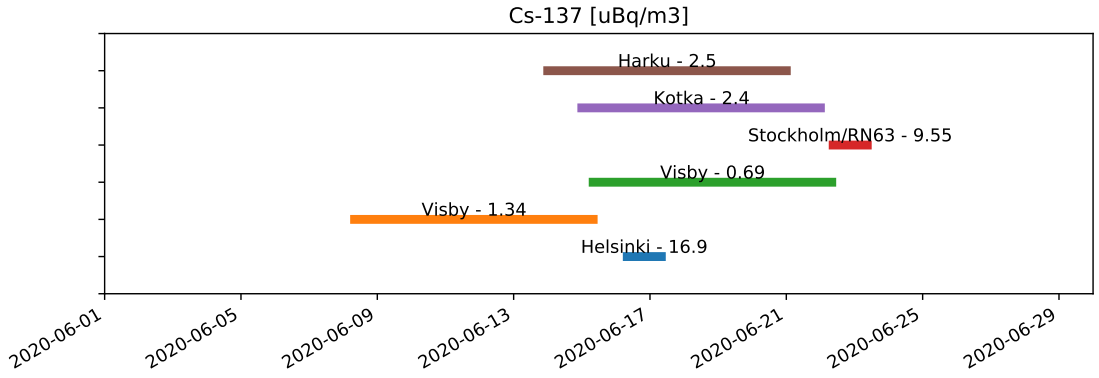

Figure 1.7: Distribution of Cs-137 measurements in the month of June 2020.

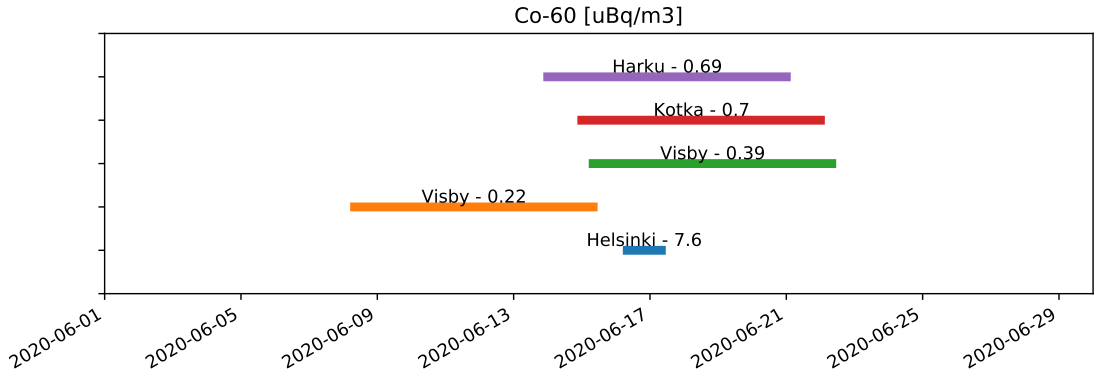

Figure 1.8: Distribution of Co-60 measurements in the month of June 2020.

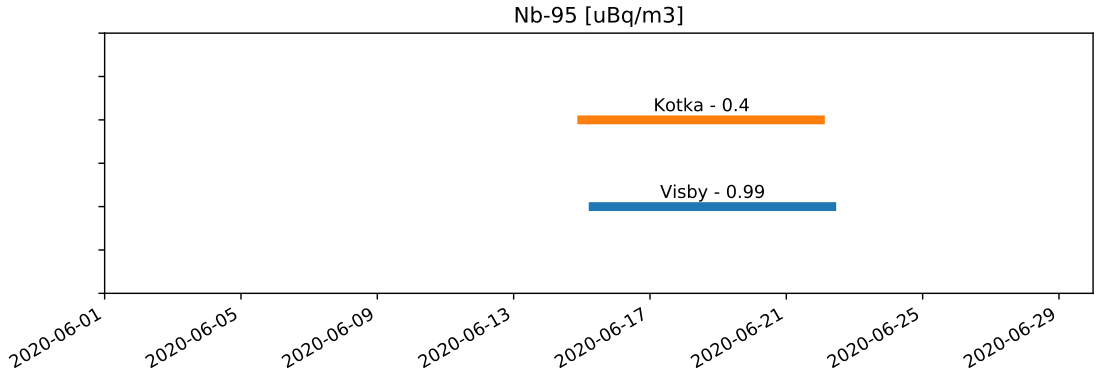

Figure 1.9: Distribution of Nb-95 measurements in the month of June 2020.

by the neutron fission reaction) might be explained assuming that Ru-106 was indeed present in the atmosphere together with Ru-103, but at values well below the minimum detectable concentration (MDC) for that nuclide.

There are only two measurements of Zr-95 (Figure 1.4), and one corresponding Ce-141 measurement (Figure 1.5), all of them with a collection period of one week. The concentrations are very low for all these isotopes, and probably present but below MDC in the other locations.

Cs-134 (Figure 1.6) was spotted at the same locations and periods of Ru-103, while Cs-137 measurements (Figure 1.7) are far more numerous. This is expected due to the very long half-life of Cs-137 and the large amounts that were dispersed and unevenly deposited over Europe after the Chernobyl incident[4].

Finally Co-60 (Figure 1.8) and Nb-95 (Figure 1.9) have been observed in small quantities in many locations. The Co-60 measurement in Helsinki is the only one that is significantly above the MDC.

2 Isotopic ratios

Isotopic ratios can be exploited to identify the type and the age of the possible nuclear fuel from which the measured material has been released[5]. Given the measurements described in Chapter 1, a few couples of isotopes have been analyzed:

- Ru-103 and Ru-106 are different isotopes of the same element, so their chemical and physical behavior is the same. Furthermore, their half-lives are relatively short and the ratio of their half-lives is almost 10, so their concentration ratio evolves significantly in time after the discharge;
- Zr-95 and Ce-141 belong to the same chemical class in the MELCOR database, meaning that they show similar behavior, have similar release fraction and follow similar release paths in the event of an accident. Their half-lives are short and the ratio of those half-lives is significantly different from 1;
- Cs-134 and Cs-137 are, similarly to Ruthenium, different isotopes of the same element. Their half-lives are significantly different with a ratio of about 1/15. Their half-lives, however, are quite long when compared with the typical times of the atmospheric simulations in the following chapters, so their relative concentration ratio does not evolve significantly in that time frame.

Short-lived isotopes, such as Ru-103, Ru-106, Zr-95 and Ce-141, reach equilibrium early during their burn-up in the reactor. Their ratios are therefore useful to know how much time has elapsed from the shutdown, since the starting value of the ratio is determined by the reactor type and the fuel cycle. The concentration of long-lived isotopes, such as Cs-134 and Cs-137, build up during the burn-up but do not reach equilibrium because their decay is slow. They can be helpful in identifying the reactor type and the fuel cycle to which they belong, because the effective amount of each of the isotope is connected to the specific fuel and operating conditions.

The ORIGEN-ARP module of SCALE 6.2.4[6] was used to evaluate the activity inventory of a fuel assembly at each End of Cycle (EoC) of a RBMK-1000 and VVER-1000 reactor for the radionuclides of interest. Table 2.1 reports the parameters adopted to perform the burn-up analysis of the two types of reactors up to EoL conditions, using a dedicated set of cross-sections for each of them.

The isotopic ratios at shutdown for each cycle and reactor type can be seen in Table 2.2. After each cycle, a decay curve is also evaluated with ORIGEN-ARP for the following 30 days. This curve is afterwards extrapolated to match the range deduced by the measurements ratios.

Table 2.3 reports the values of these ratios computed with their uncertainty propagating the original uncertainties of the measurements. The uncertainty is here defined

Table 2.1: Set of parameters for ORIGEN ARP calculation — SCALE 6.2.4

physical quantity	VVER-1000	RBMK-1000	unit of measure
thermal power	3000	3200	MWth
FA burn-up (discharge)	50200	23000	MWd/MTU
specific thermal power	42.55	16	MWth/MTU
enrichment	4.95	2.1	wt%
moderator density	0.723	0.50	g/cc
number of cycles	3	3	–
number of libraries per cycle	1	1	–
number of days per cycle	333	479	day
decay time after each cycle	30	30	day

Table 2.2: Isotopic activity ratios at shutdown.

ratio	reactor type	Cycle I	Cycle II	Cycle III
Ru-103 / Ru-106	VVER-1000	7.92	4.14	2.99
	RBMK-1000	5.76	3.20	2.41
Zr-95 / Ce-141	VVER-1000	1.05	1.04	1.01
	RBMK-1000	1.06	1.03	0.99
Cs-134 / Cs-137	VVER-1000	0.58	1.11	1.53
	RBMK-1000	0.34	0.65	0.92

Table 2.3: Isotopic ratios from measurements.

ratio	location	date	value	rel. uncertainty
Ru-103 / Ru-106	Visby	22	0.493	0.500
Zr-95 / Ce-141	Kotka	22	1.000	0.269
Cs-134 / Cs-137	Helsinki	17	1.302	0.103
	Visby	15	0.575	0.078
	Visby	22	0.884	0.122
	Stockholm	23	1.012	0.136
	Kotka	22	0.708	0.064
	Harku	21	1.120	0.072

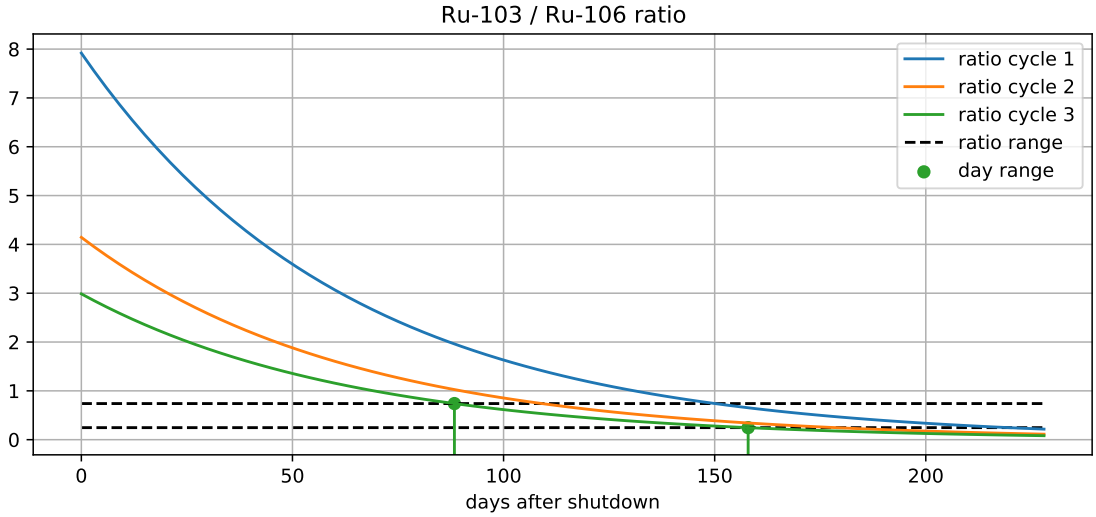

Figure 2.1: Ru-103 over Ru-106 ratio for a VVER-1000.

as 1 standard deviation away from the mean value. There is only one isotopic ratio available for the Ru-103/Ru-106 and Zr-95/Ce-141 couples. Many more suitable couples are available for the couple Cs-134/Cs-137, but the value of the ratios vary sensibly from measurement to measurement, in a time period that does not justify such a variation due solely to radioactive decay. Cs-137 measurements, however, can contain resuspended material coming from the 1986 Chernobyl incident, that is still present unevenly over Europe due to its very long half-life[4]. This Cesium can affect the measurements and we will try to address this issue in Section 2.3.

2.1 Ru-103 and Ru-106 ratio

Figure 2.1 shows the evolution of the decay curve after shutdown for all 3 cycles in a VVER-1000. The dashed lines represent the estimated value of the ratio of Ru-103 and Ru-106 for the measure in Visby that contained both isotopes that gives a value of 0.493 ± 0.247. This ratio is compatible with fuel discharged at each cycle, with a time after shutdown varying from about 80 days up to about 220 days. In case of fuel that has undergone 3 cycles in the reactor, the estimated time range after shutdown would be 88 to 158 days, as shown by the green markers in the figure.

Figure 2.2 reports the same evolution for a RBMK-1000. The overall behavior is quite similar to the VVER-1000 case, with an estimated range between about 75 and 200 days. In case of fuel from Cycle III, the range would be 75 to 144 days, as shown in the figure.

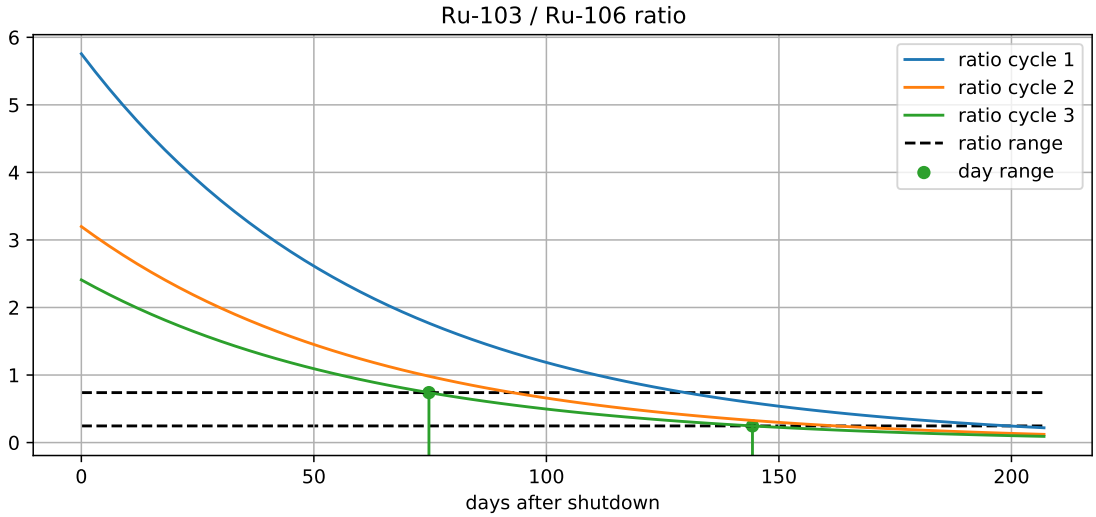

Figure 2.2: Ru-103 over Ru-106 ratio for a RBMK-1000.

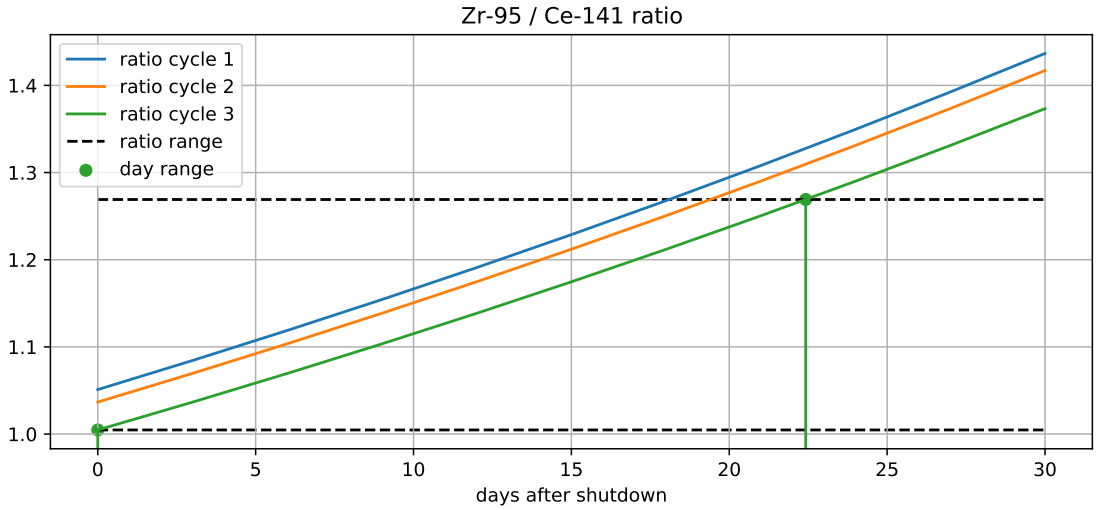

Figure 2.3: Zr-95 over Ce-141 ratio for a VVER-1000.

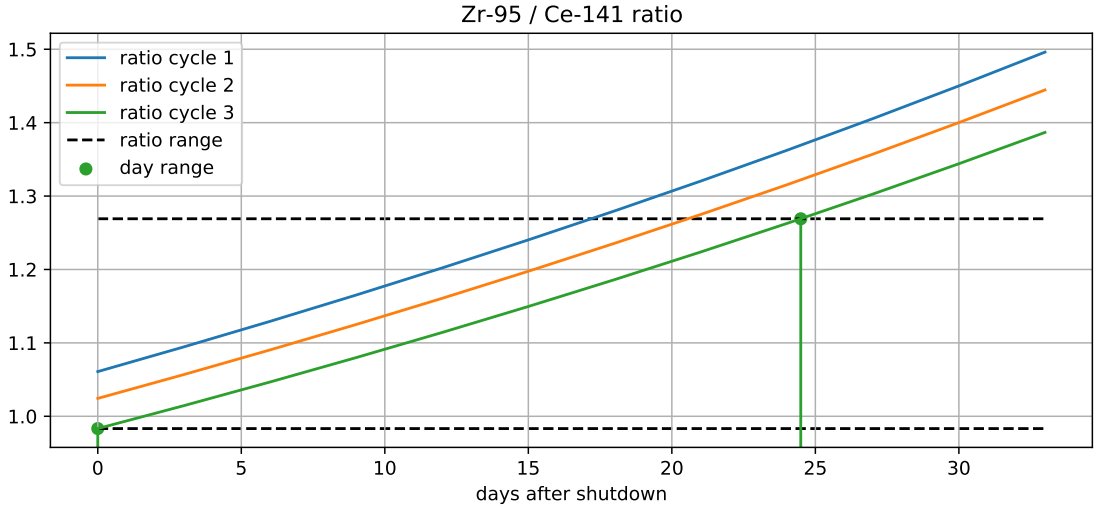

Figure 2.4: Zr-95 over Ce-141 ratio for a RBMK-1000.

2.2 Zr-95 and Ce-141 ratio

There is only one measurement of Ce-141 among the anomalous ones registered in June 2020, and it is coupled to a Zr-95 one. The ratio of their concentration is 1.00 ± 0.27. The comparison of this range with the decay curve for this isotopic ratio is shown in Figure 2.3. The decay curves predict a ratio that starts at about 1 and that grows in time, as Ce-141 decay twice faster than Zr-95. This gives an estimated time range that starts right at shutdown and is anyway smaller than about 23 days. In particular, as reported in the figure, the time range for Cycle III would be 0 to 22.5 days.

The situation for an RBMK-1000 is shown in Figure 2.4 and is substantially the same as for the VVER-1000. The ratios at shutdown are a little bit more spread apart, but the deduced time range is anyway included between 0 and about 25 days. For Cycle III, the time range would be 0 to 24.5 days.

2.3 Cs-134 and Cs-137 ratio

As we have already pointed out, the isotopic ratios in Table 2.3 vary significantly among sites and measurements. The theoretical ratio of Cs-134 and CS-137 does not change significantly on the time scale of some month due to the isotopes' half-lives.

Even taking into account the provided uncertainty, it is difficult to have a clear picture of where to set the ratio for the Cesium isotopes from the available data. In particular, if the only two measurements made over a single day (the one in Helsinki and the one in Stockholm) have to be trusted, the isotopic ratio is predicted to be greater than 1. The Harku measurement also agrees with this picture. In this scenario, the RBMK-1000 could be excluded due to the ORIGEN-ARP calculated ratios that stay below one at

all times due to the typical lower burn-up values at EoL. The VVER-1000 curves would indicate that the fuel is from Cycle II or most probably Cycle III.

However, Visby and Kotka measurements do not allow for a ratio above one. The apparent discrepancy can be partially justified by the presence of Cs-137 in the air samples from different sources, namely the resuspension of Cs-137 from the 1986 Chernobyl accident. For Visby, the laboratory suggests that a suitable value of background Cs-137 would be $(0.4 \pm 0.2)\,\mu Bq/m^3$. With this background, the measurements can be assumed to be $(0.819 \pm 0.192)\,\mu Bq/m^3$ and $(2.103 \pm 1.541)\,\mu Bq/m^3$. The first value is still smaller than one, even at the top of its variability range, while the second becomes highly uncertain due to its low absolute value.

3 Backward and forward trajectory analysis

This chapter is devoted to the analysis of the backward and forward trajectories of the air masses on the location and time of the most relevant measurements reported in Chapter 1 in order to assess a possible origin of the release and the correlation among the different measurements.

The backward tracking of the air masses using the mean wind alone (disregarding the turbulence in the atmosphere) is an efficient and quick way to pinpoint a possible region of origin for the release that produced the aforementioned measurements.

Based on the results obtained with these simulations, all the relevant nuclear site locations of the predicted source have been visualized in Figure 3.1. The numbering used there will be the same for both this chapter and Chapter 4.

All the simulations shown in this chapter have been performed using HYSPLIT 5.0.0[7, 8] with meteorological data provided by the *Global Forecasting System (GFS)* from NOAA at a resolution of 0.25° in space and an update frequency of 3 hours.

3.1 Helsinki

The first measure that has been communicated is the one from Helsinki. The backward trajectories of the air masses for the period of the measure can be seen in Figure 3.2. The color of the trajectory changes from blue to red as the time moves backwards. In this simulation, one trajectory is started at every hour along the 24 hour span of the measurement.

It can be seen that the trajectories are fairly consistent among each other, highlighting that the atmosphere in the region was quite stable for the period of interest. The largest part of the trajectories travel eastwards for some time and afterwards the trajectories veer towards south-east for an extended section. After about two days of backward motion, the trajectories take an anti-clock-wise motion that leads to north bound trajectories in the final stage of the simulation. Some trajectories initially separate from the others and travel a bit west, but, they soon take the same anti-clock wise spin as the others and they mostly join back with the others after about 3 days of simulation.

The region spanned by these trajectories cover the Baltic countries and the western side of Russia, where many nuclear power plants are located. This simulation has been in fact used to select the relevant nuclear power plants listed in Figure 3.1.

Figure 3.3 shows the forward trajectories of the air masses over Helsinki relative to the measure that has been analyzed in the previous part. The trajectories in this case are colored based on the age of the particles, i.e. the amount of time that has passed since their release in Helsinki. The color change from day to day in the sequence: blue, cyan,

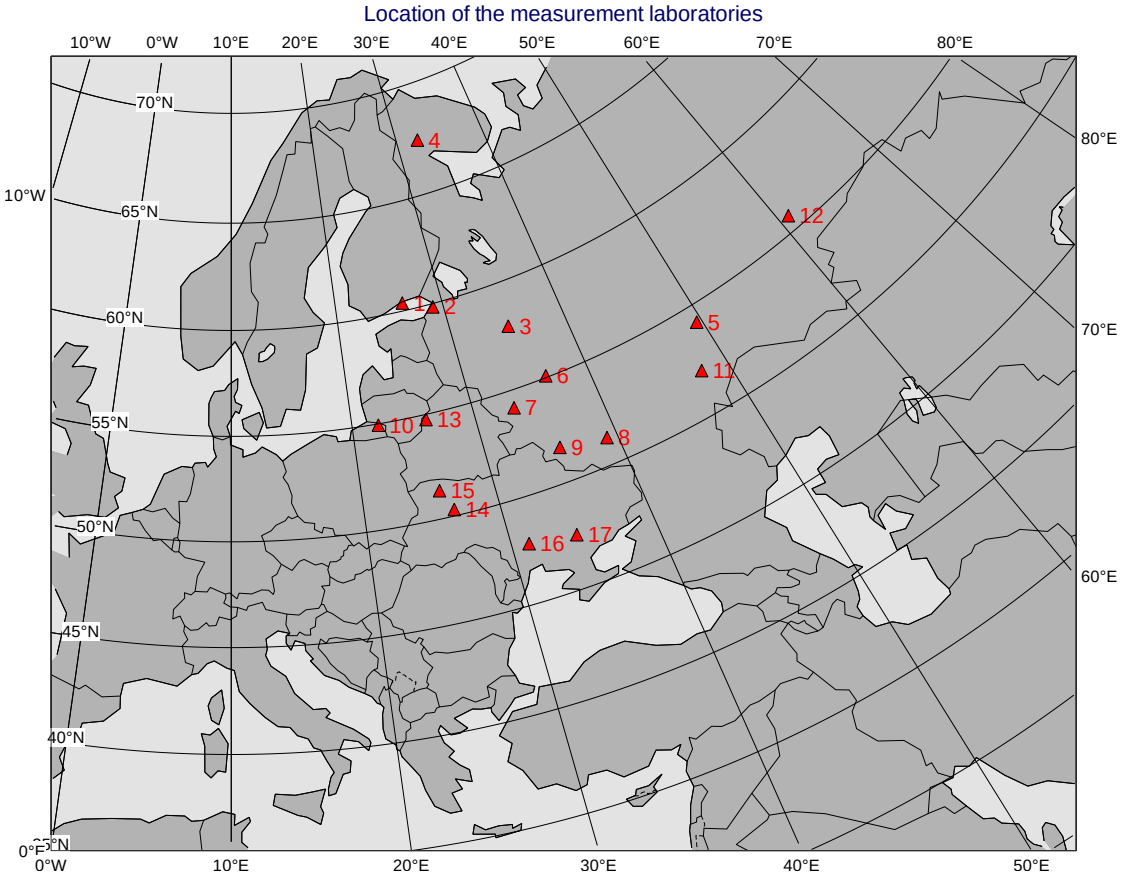

id	name	type	latitude	longitude
1	Loviisa	VVER-440	60.37	26.35
2	Leningrad	RBMK-1000	59.85	29.04
3	Kalinin	VVER-1000	57.91	35.06
4	Kola	VVER-440	67.47	32.47
5	Dimitrovgrad	BOR-60, Reprocessing	54.18	49.58
6	Obninsk	Shut down	55.08	36.57
7	Smolensk	RBMK-1000	54.17	33.25
8	Novovoronezh	VVER-440/1000/1200	51.28	39.20
9	Kursk	RBMK-1000	51.68	35.61
10	Kaliningrad	Under construction	54.94	22.16
11	Balakovo	VVER-1000	52.09	47.96
12	Mayak	Reprocessing	55.71	60.85
13	Astravets	Under construction	54.76	26.09
14	Khmelnytskyi	VVER-1000	50.30	26.65
15	Rivne	VVER-440/1000	51.33	25.89
16	South Ukraine	VVER-1000	47.82	31.22
17	Zaporizhia	VVER-1000	47.51	34.59

Figure 3.1: Relevant nuclear installations.

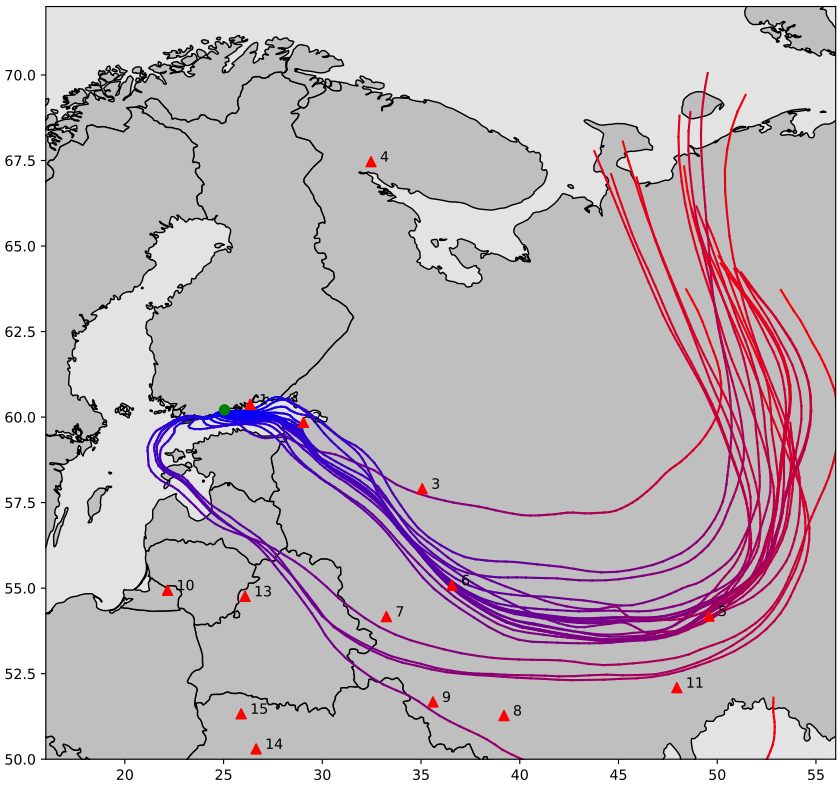

Figure 3.2: Backward trajectories from Helsinki for 5 days.

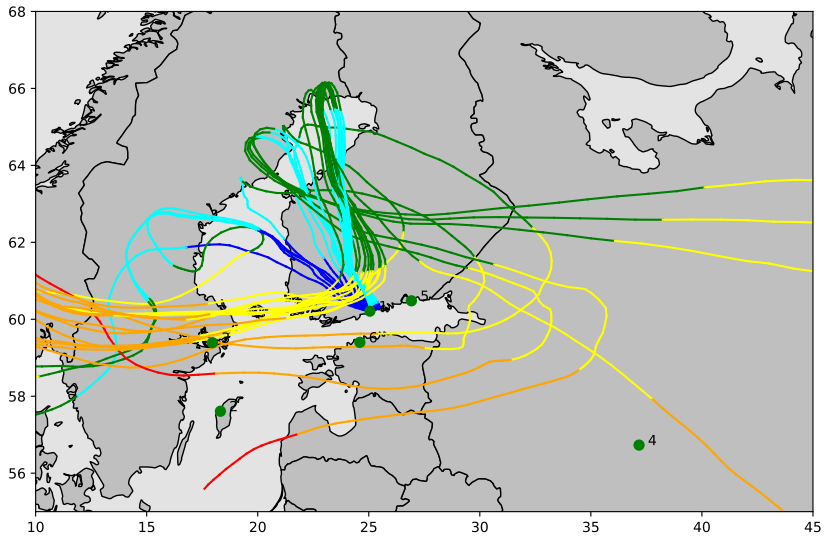

Figure 3.3: Forward trajectories from Helsinki for 7 days.

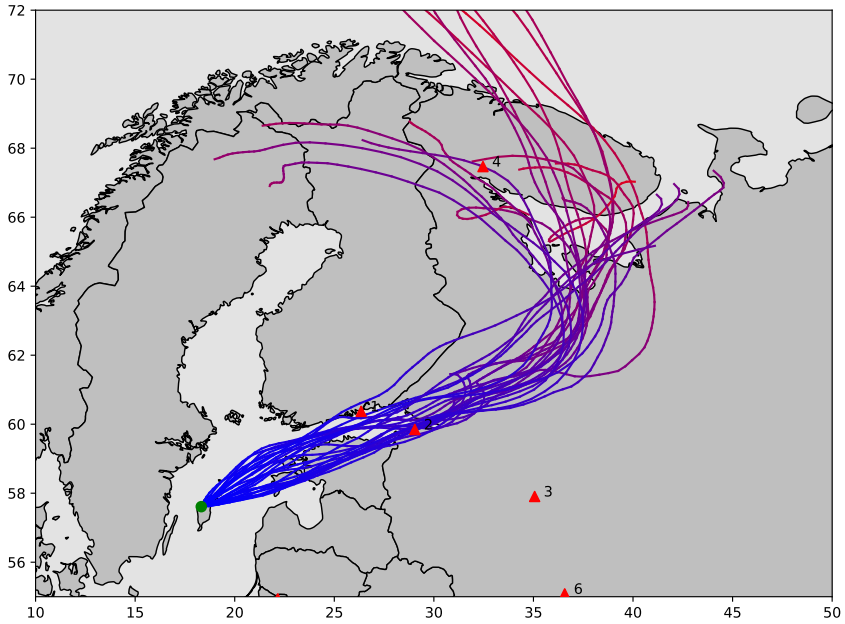

Figure 3.4: Backward trajectories from Visby for 5 days (3 days measure on the second week of June).

green, yellow, orange, red, purple (that is completely only present outside the boundary of the picture as shown here).

We can see that the most of the trajectories take a recirculation pattern over Finland that spreads for more than three days. Afterwards, the air masses travel westwards to Scandinavia and they reach Stockholm in about five days. This amount of time is compatible with the anomalous measurement in Stockholm between the 22nd and the 23rd. This seems to indicate that the two measurements are related to each other, or in other words that the radionuclides that have been collected belong to the same cloud.

The trajectories are compatible also with the Visby and Kotka measurements, but these ones are over a much longer collection time, so these connections are less informative.

3.2 Visby

Figure 3.4 shows the backward trajectories for the air masses above Visby in the period of the first measure that was registered in the second week of June. In order to reduce the variability of the results, it has been considered only a 3 day period for the measure, instead of the real period of 7 days. The 3 days are the final days of the measurement period, the closer ones to the measure in Helsinki. In this case the backward emission is of one trajectory every three hours, so to get 24 trajectories in total similarly to Helsinki. Also in this case the color (ranging from blue to red) specifies the age of the trajectory.

We can see that also in this case the atmosphere is quite stable, as all trajectories travel

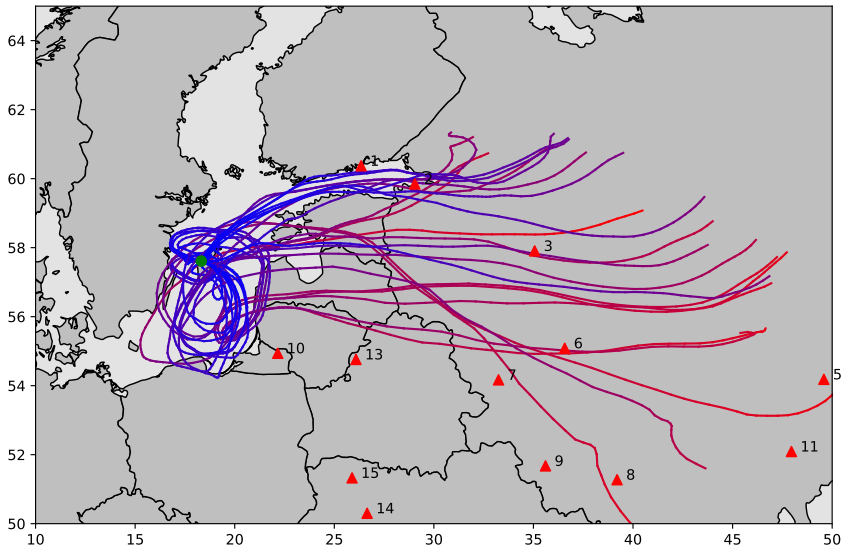

Figure 3.5: Backward trajectories from Visby for 5 days (3 days measure on the third week of June).

close to each other towards east/north-east in the first days. After about two days the trajectories deviate towards north and they end their 5-day journey well beyond the northern coasts of Scandinavia. In fact, the final part (in red) of many trajectories is not displayed here as it goes northern and northern.

It can be noted that the trajectories from Visby travel above the Kola NPP (n. 4 in the map), while the Helsinki ones did not. In fact, from the simple analysis of the air mass trajectories the only two common NPPs are the Loviisa NPP (n. 1) and the Leningrad NPP (n. 2). The timing, however, do not cohincide in the two simulations, as we will see in the next chapter when we will look at backward concentrations.

Figure 3.5 shows the simulation for the second measurement in Visby that happened in the third week of June, with the same assumptions and visualization as the previous one that we have seen previously. The backward emission period of three days encompasses completely the measurement in Helsinki.

The trajectories show a recirculation pattern that develops in the first two days of simulation, that keeps the air masses in very close proximity to Visby, differently from the other case. This is in agreement with Figure 3.3 that we have seen in the previous section. After this recirculation period, the back-trajectories move eastwards and spread across all the eastern margin of Russia.

These trajectories are only partially overlapping with the ones from the previous week that we have seen in Figure 3.4, as they travel further south than the others. The spread among them is quite larger than before, probably due to a more unstable weather condition connected to the recirculation loop that develops in the first part of the simulation.

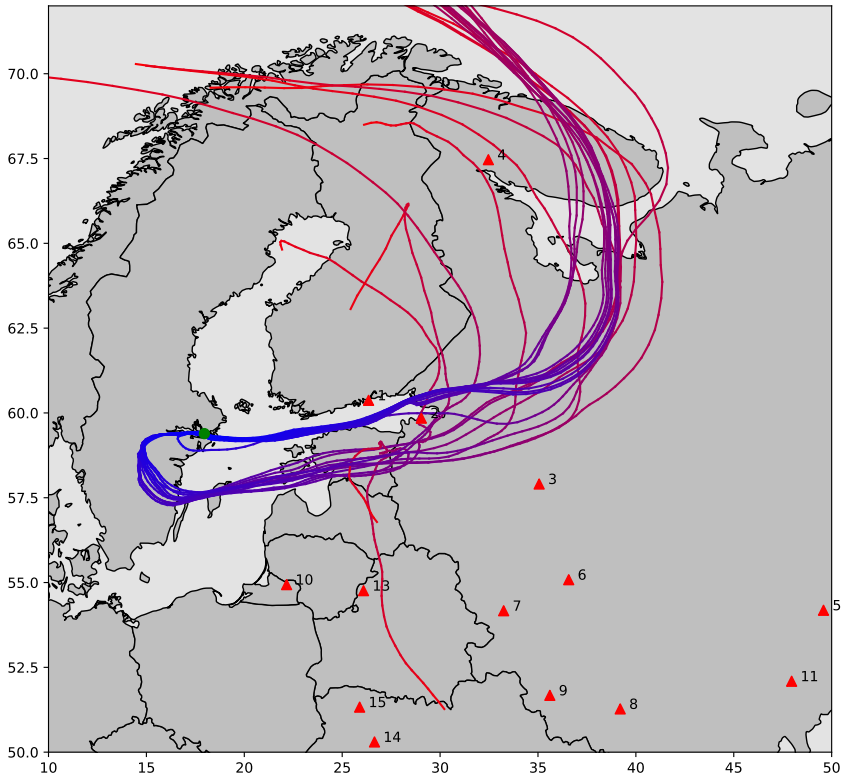

Figure 3.6: Backward trajectories from Stockholm for 5 days.

3.3 Stockholm

The anomalous measurements in Stockholm were registered almost a week later than the first ones from Helsinki and Visby, but the identified isotopes were the same. In Figure 3.6 we can see the backward trajectories of the air masses over Stockholm in the period of the measure.

In this case, there is a net separation in two different clusters of trajectories, one moving eastwards and the other moving westwards from Stockholm. The one moving west, however, soon turns anti-clockwise and proceeds eastwards as the other. Due to this initial discrepancy, the two clusters reach the same regions at different times (as visualized by the different color of the trajectories in the same places) and finally turn northbound similarly to what we have seen previously.

Given the difference in time of the measures, it can be seen that the atmosphere is still fairly stable for the whole period, as all the trajectories travel towards the same region. This, together with the fact that the isotopes that were observed are the same in all the laboratories, indicates that the source of the release is the same for all of them. Due to the spatial closeness of the laboratories, however, no clear indication of the specific location of the release can be inferred by the backward trajectories analysis.

4 Backward concentration analysis

In this chapter we will analyze backward concentration simulations for the same measurements that we have reported in Chapter 3 and some additional ones that have been included to better understand the sensitivity patterns.

The concentration simulations are more computationally intensive with respect to the trajectory simulations, but they give richer information on the possible origin of the measured concentration since they take into account for the turbulence in the atmosphere. In particular, these simulations output the source-receptor-sensitivity (SRS) probability (measured in s^{-1}) that links each point on the grid to the measurement site. While these probabilities cannot be used and compared based on their absolute values, they can be useful in relative comparisons and especially when combining multiple simulations that, when the starting measurements are well behaved (see Section 1.3), can pinpoint the origin of a release satisfying all the constraints simultaneously[9]. This approach is particularly useful in matching concentration clouds that cover similar regions of space but at different times, as we will see in the following.

All the simulations in this chapter have been performed with FLEXPART 10.4[10, 11, 12, 13, 14, 15], using forecast and analysis meteorological data of the HRES atmospheric model from the *European Centre for Medium-Range Weather Forecast (ECMWF)*, with a spatial resolution of 0.25° and an update frequency of 3 hours. The possible source nuclear sites are the same of the previous chapter, as illustrated in Figure 3.1.

4.1 Helsinki

Figure 4.1 shows the SRS for the backward simulation based on the Helsinki measurements. The pictures frames are taken at 12:00 UTC on the days starting from the 16th and going back to the 10th. The probability cloud follows a similar path to the trajectories that we have seen in Figure 3.2.

The first frame is taken when the release is still ongoing, while starting from the second frame we can see that the cloud detaches from Helsinki and it starts traveling south east. We can see that the peak of the probability follows the same anti-clock-wise motion as we have seen for the trajectories, but after about 4 days the cloud develops two distinct maxima.

Anyhow, the probability associated with the nuclear sites annotated in the map that are located in western Russia and adjacent countries is significantly different from zero when taking into account for this measurement alone. The only place that is outside the probability cloud for a significant amount of time, before the cloud spreads almost evenly in the last frame, is the Scandinavian region and the Kola NPP.

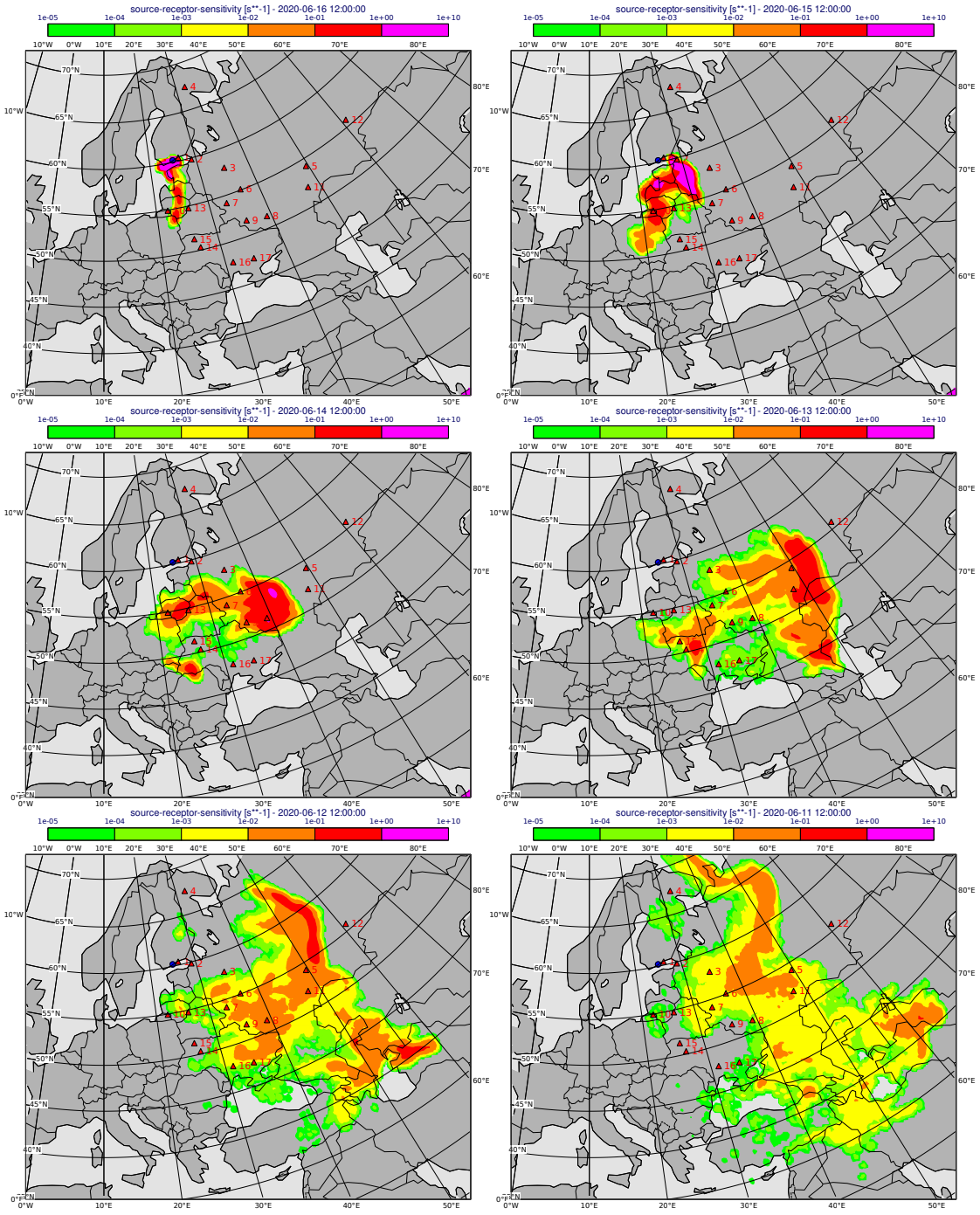

Figure 4.1: Backward concentrations for the measurement in Helsinki.

4.2 Visby

For what concerns the backward concentration simulations based on the Visby measurements, two different hypotheses have been followed:

6d Restrict the measurement period to three days instead of seven. This is useful to reduce the spread of the probability cloud and get better information. The hypothesis is that the cloud has reached Visby in the six day period that crosses evenly the two weeks of measurements with anomalous values.

14d Use the full two week range dictated by the measurements. This is useful to understand how the previous hypothesis affects the results and if it can be considered for further analysis. This is especially important since reducing to six days reduces the computational time by a factor of more than 3, due to the possibility to reduce the number of particles used and the smaller time frame that is required to simulate.

In Figure 4.2 we can see the same frames that we have seen for Helsinki for the **6d** case. Also in this case we can see that the behavior of the core part of the cloud is similar to the trajectories that we have seen in Figure 3.4 and Figure 3.5, that have been performed with the same hypothesis.

The part of the probability cloud with higher SRS values travels eastward after recirculating over the backward emission area. The cloud is located over western Russia, but it seems to exclude other nuclear sites in other countries further west. The higher probability regions are all located above the 55°N parallel.

Figures 4.3, 4.4 and 4.5 show the simulation in the **14d** case. The simulation is much longer in time, requiring many more frames to be shown. Figure 4.3 shows the days starting from the 22nd and backwards to the 17th. Figure 4.4 has the same days as the case of Helsinki and **6d** for a direct comparison between images. Finally, Figure 4.5 reports the frames for the days from the 10th the the 5th.

It is clear that this simulation is quite noisier than the previous one due to the longer simulation time that promotes the spread of the cloud due to the atmospheric turbulence. If we compare the frames at the same instant between the **6d** and **14d** cases, we can see that the reduced case captures correctly the behavior of the bulk of the SRS cloud. There is only an initial peak located in the south-west of Russia, that is produced by the early part of the release and that therefore cannot be present in the **6d** case.

4.3 Stockholm

Figure 4.6 shows the backward simulation based on the measurements in Stockholm. The time frames shown go from the 22nd to the 17th. Also in this case the behavior of the cloud is similar to the back-trajectories we have seen in Figure 3.6. The peak of the cloud is over north-west Russia and it travels north from there. The most probable locations that could have originated this measurement are the NPPs located near the Baltic Sea on the nuclear site of Kola.

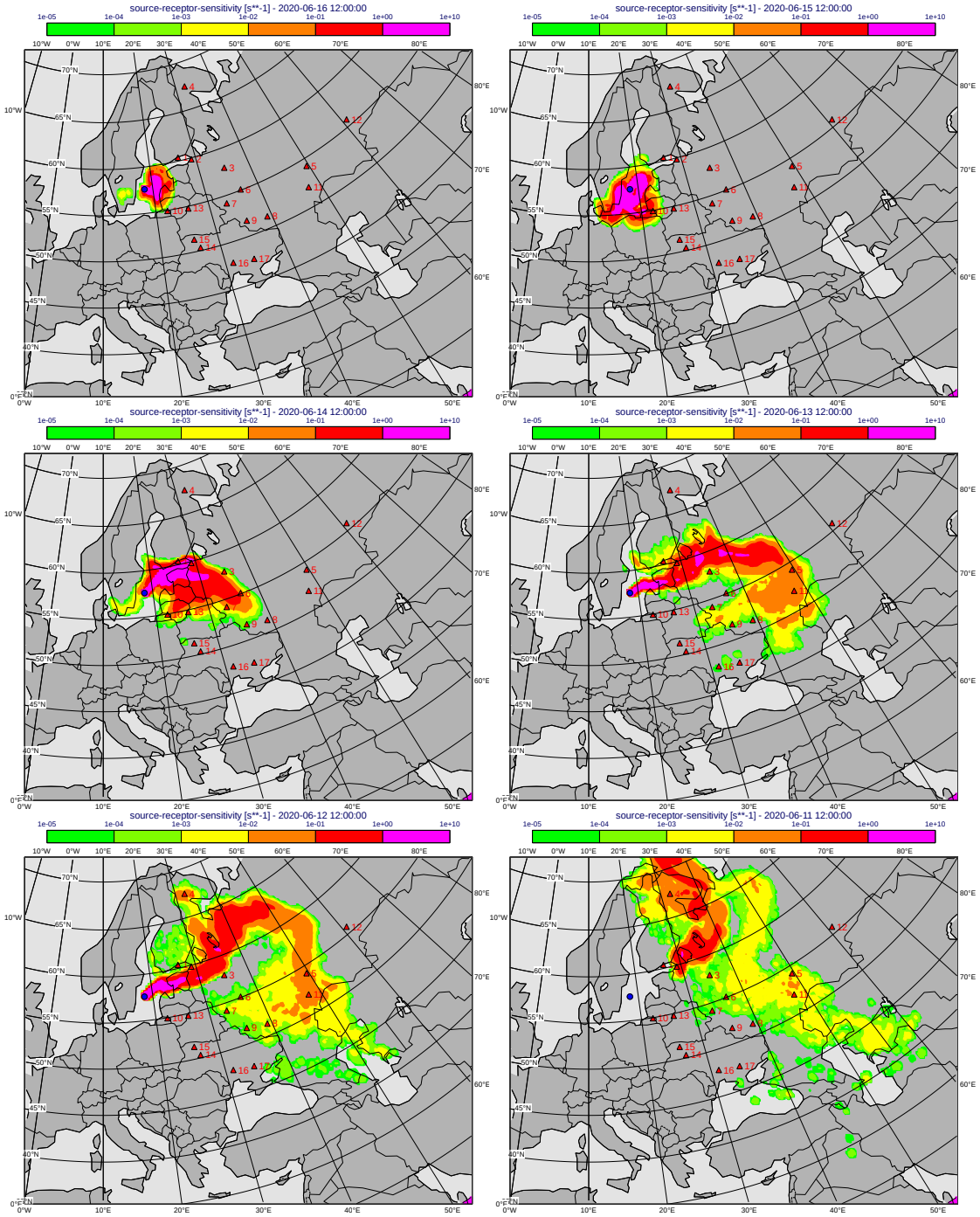

Figure 4.2: Backward concentrations for the measurements in Visby (3 + 3 days emission).

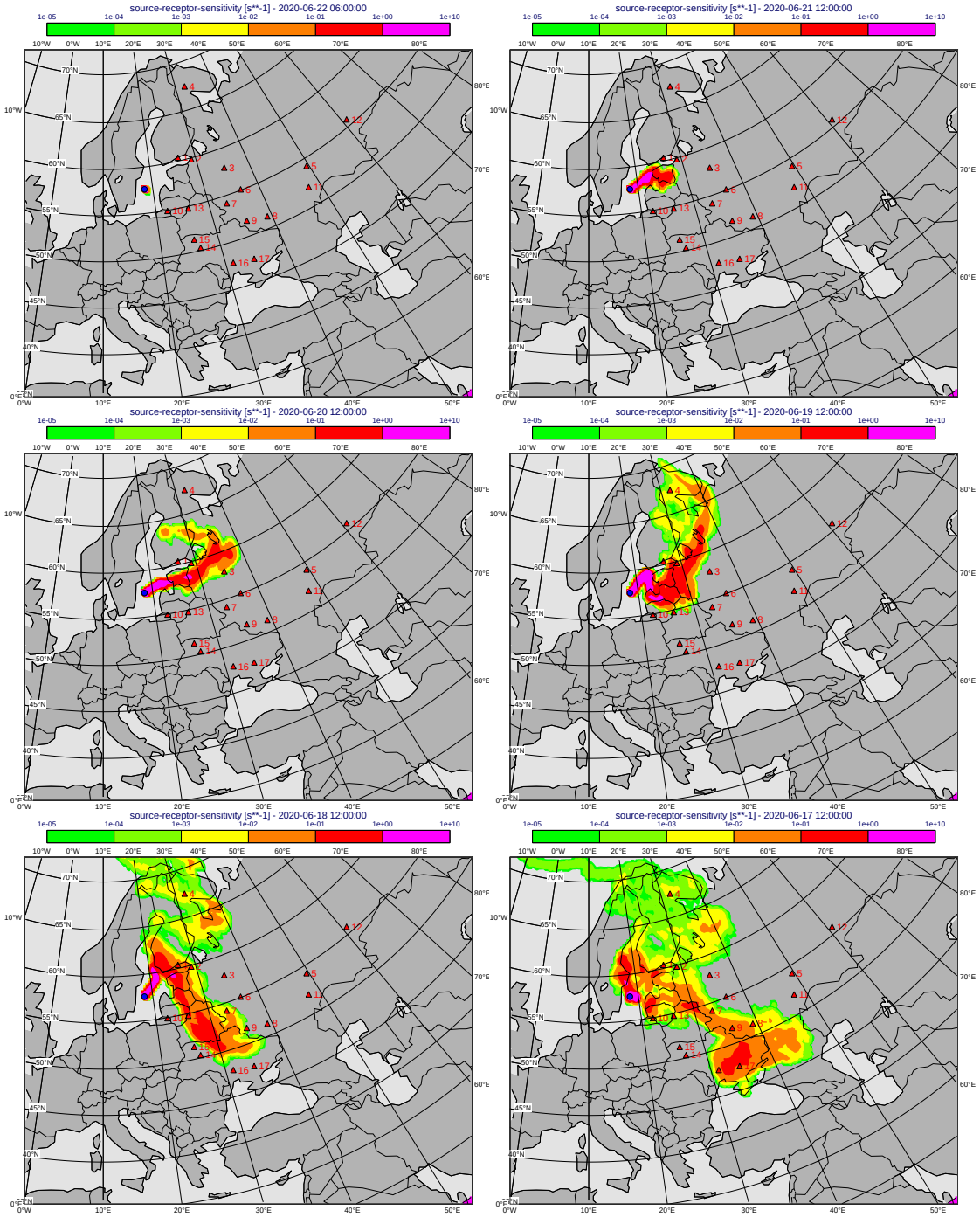

Figure 4.3: Backward concentrations for the measurements in Visby (7 + 7 days emission).

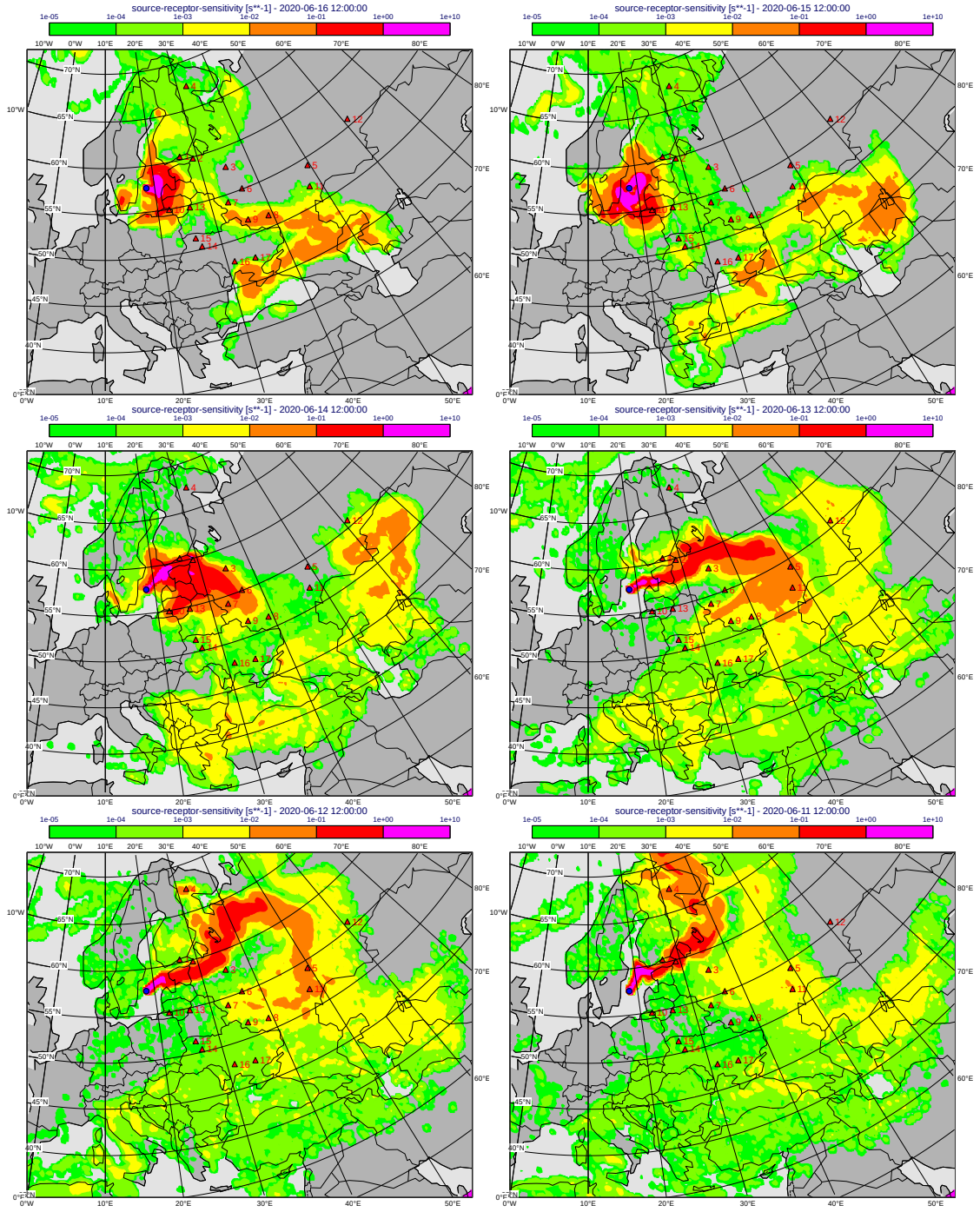

Figure 4.4: Backward concentrations for the measurements in Visby (7 + 7 days emission).

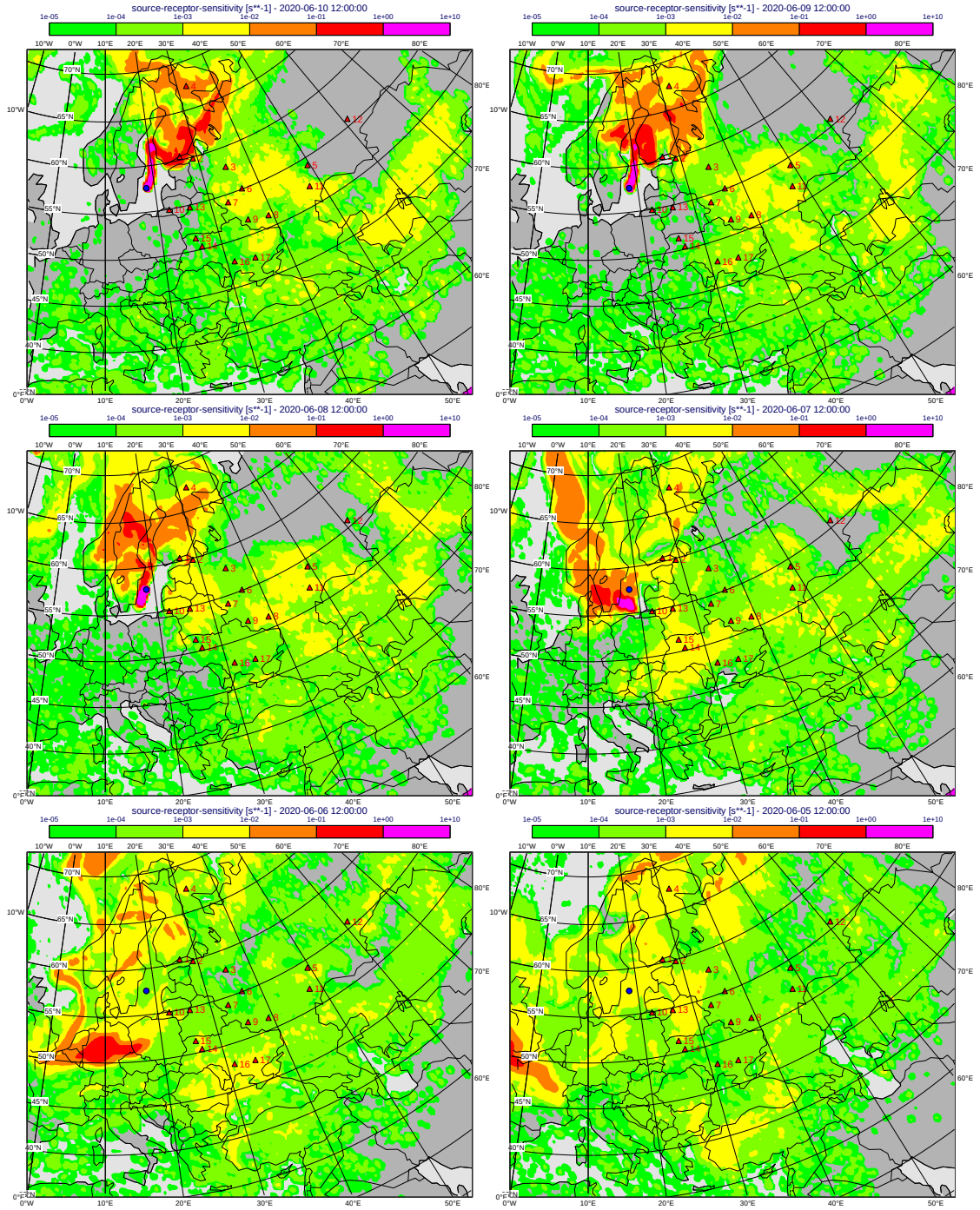

Figure 4.5: Backward concentrations for the measurements in Visby (7 + 7 days emission).

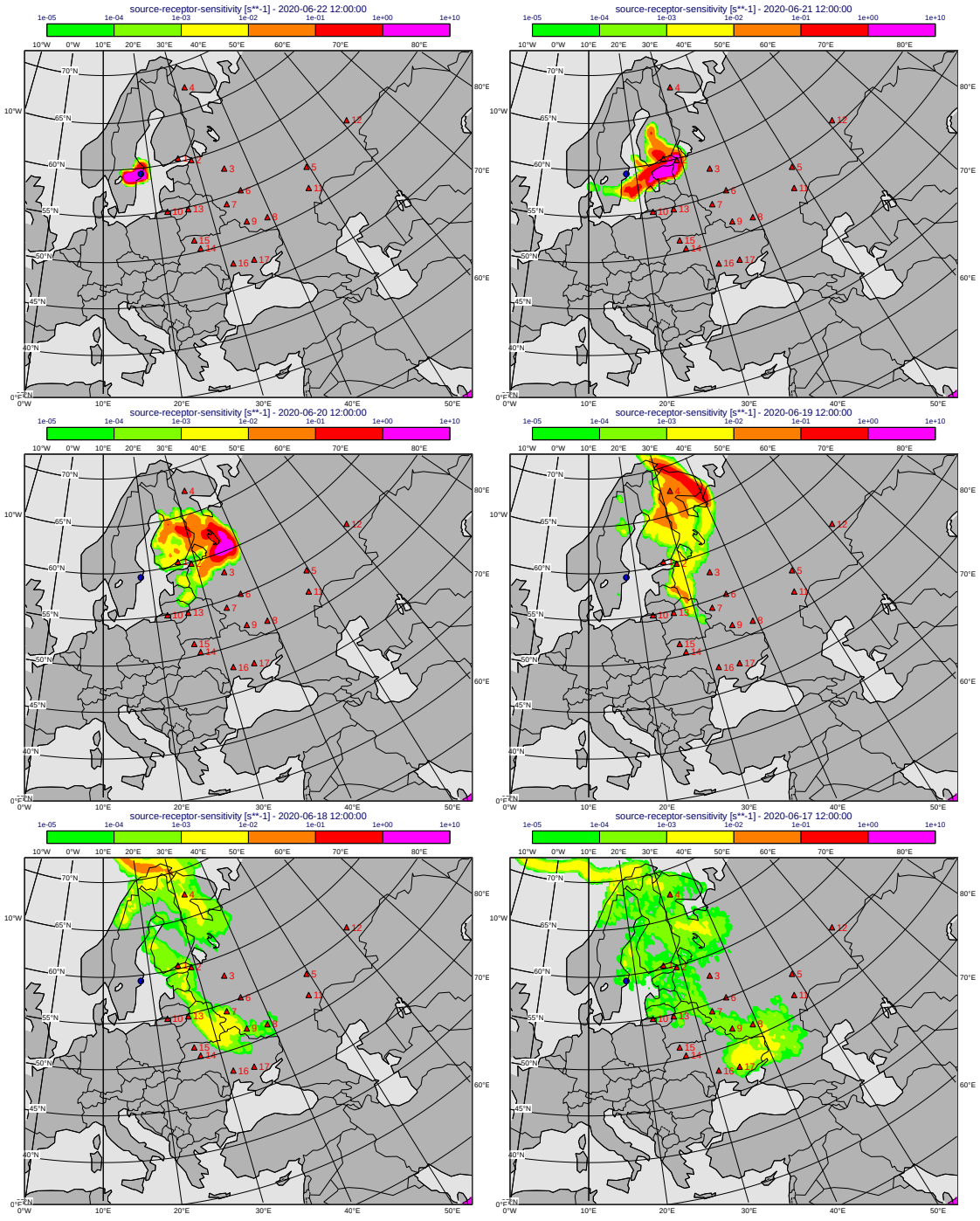

Figure 4.6: Backward concentrations for the measurement in Stockholm.

A second smaller peak is present over west Russia and Ukraine, but it is comparatively smaller then the other one. Already at the latest frame shown here, on the 17th, the cloud is quite spread over a large region. The other measurements that we have seen before start after this date, leading to a scarce capability of integration with the other measurements as we will see in the next section.

4.4 Combined simulations

One of the greatest advantage of using backward concentration simulations is that they can be easily integrated to look at the combined SRS probability that is a visual representation if the probability that a given point of the grid can simultaneously be the origin of the measurements in all the measurement backward concentrations that have been combined.

Figure 4.7 shows the combined cloud for the simulation originated in Helsinki and Visby (using the **6d** hypothesis). The combined cloud covers similar regions to the ones already analyzed for the single simulations. Unfortunately, as already introduced, the geographical closeness of the two laboratories implies that the overall behavior of the single clouds is quite similar, leading to a combined cloud that does not pin-point specific locations with spots that show up only at some limited set of times steps, but to a continuous cloud that mimics the behavior of the single clouds.

In Figure 4.8 we show the same time frames when using the Visby case **14d**. It is clear that, when combining with the Helsinki simulation, the difference between the two Visby cases is even smaller then in the single case.

Therefore, the possible origin, assuming that the measurements are the product of the same emission, cannot be easily selected by looking at the SRS combined clouds. Figure 4.9 shows the interpolated value of the combined probability cloud at the selected nuclear sites that gives a value different from zero for all time steps. In the picture, RBMK reactors are shown with a dashed line, while the continuous line is used for the VVER reactors, while the top graph is for the Visby case **6d** and the bottom graph is for the **14d** case.

The interpolated values are substantially equivalent between the two cases. The only relevant omission from the **6d** is the early peak connected to the Leningrad NPP. Overall, the **6d** case is a restriction of the **14d** case that misses the fringe part of the cloud but clearly captures the bulk behavior.

As seen from the clouds, it is not possible to isolate a clear location for the emission, even in the case that an emission time interval could be pin-pointed by other means (such as isotopic ratios). It is important to highlight that in these graphs the comparison among sites should be made only at corresponding time values, while the comparison at different time steps is less relevant as it is influenced by the age of the simulation (and therefore the amount of turbulence that has affected it).

Finally, Figure 4.10 shows the combined SRS cloud for Helsinki and Stockholm. As we can see here, the combination produces little more than numeric error. This is due to the temporal distance between the two measurements. When the Helsinki release starts, the

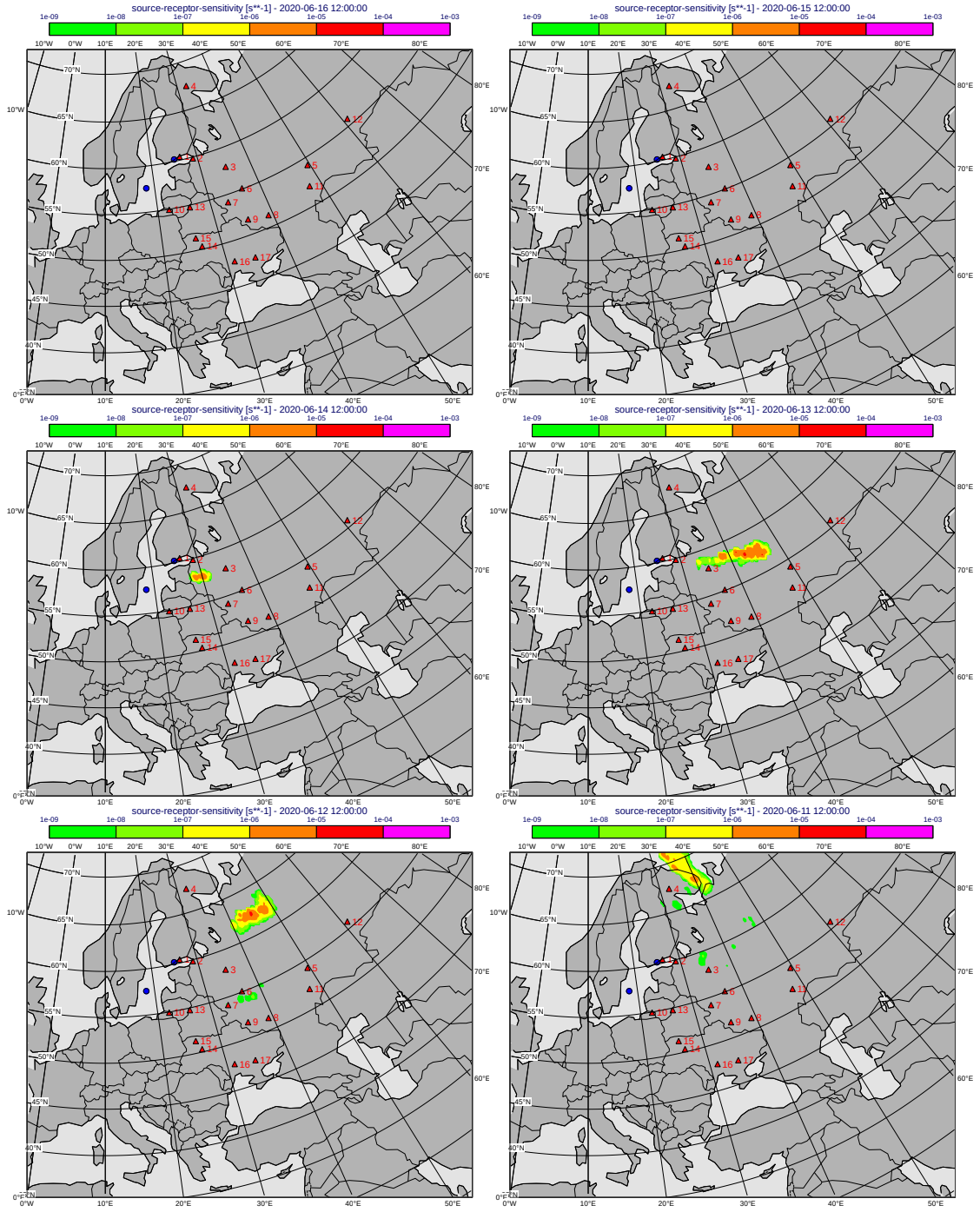

Figure 4.7: Combined backward concentrations for the measurements in Helsinki and Visby (3 + 3 days emission).

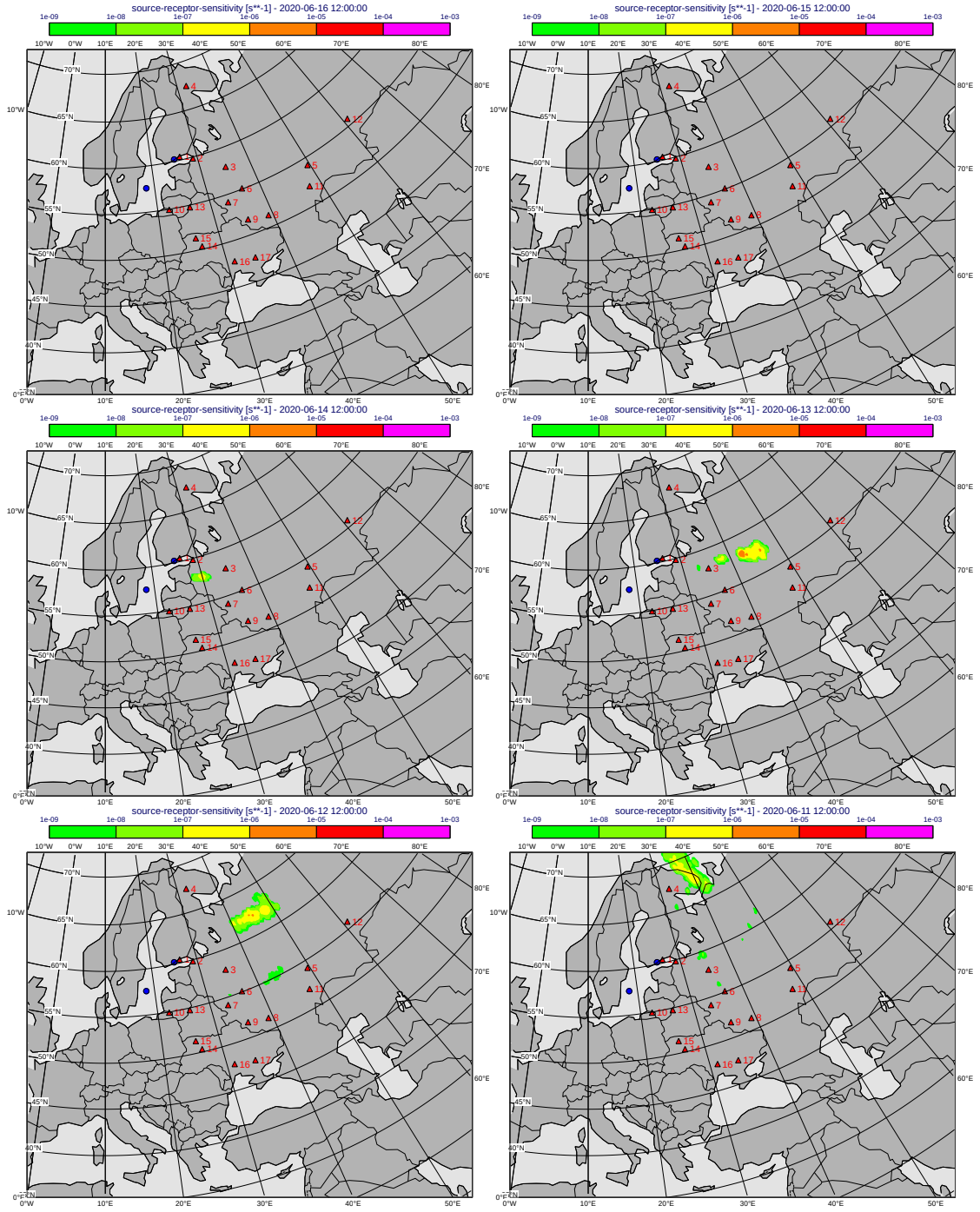

Figure 4.8: Combined backward concentrations for the measurements in Helsinki and Visby (7 + 7 days emission).

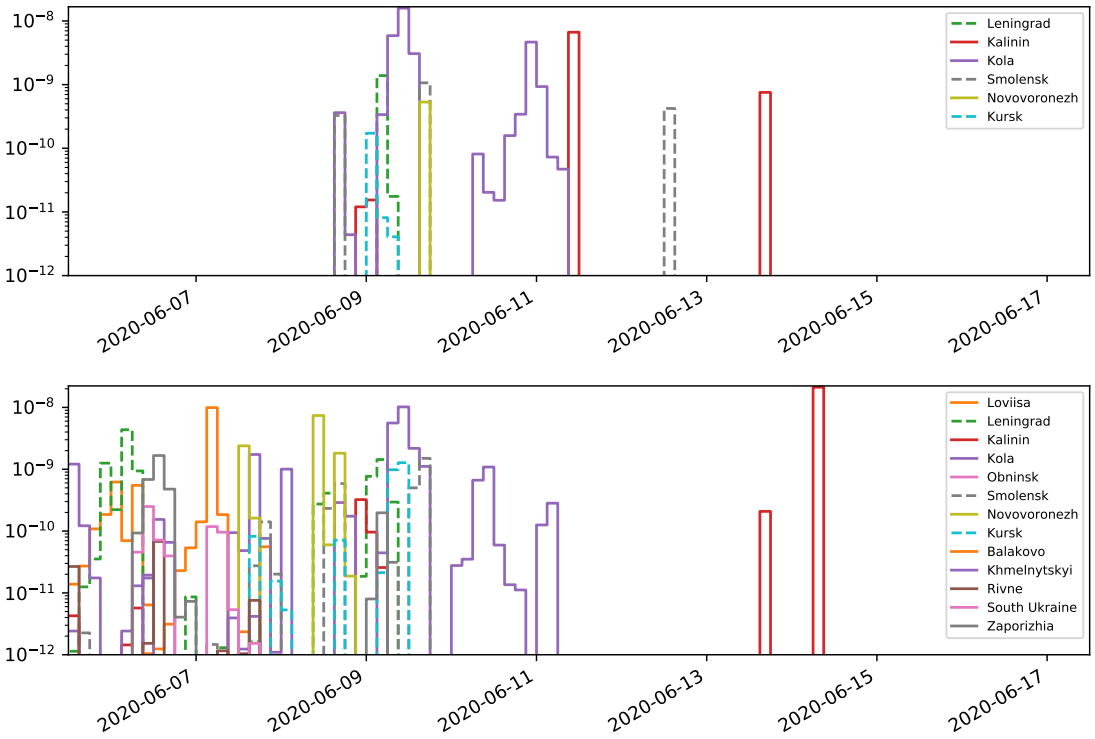

Figure 4.9: Interpolated source-receptor-sensitivity for some relevant nuclear installations.

cloud from Stockholm has already dispersed for more then six days and it is widespread on a large region with values that are already quite small. The injection from Helsinki therefore does not contribute significantly to highlight possible origin points.

4.5 Combined simulations taking into account for measurements below MDC

The absence of a measurement above the minimum detectable concentration (MDC) can be considered an information as well as its presence. In particular, when there is no measurement we can try to exclude all sources that would produce a concentration above MDC in the selected location. To this end, we can perform backward simulations with a fictitious release at the location and use the source-receptor-sensitivity as *exclusion regions*.

We can see an example of this approach in Figure 4.11, that pictures the backward concentration for the missing measurements in Helsinki. The caveat of this approach is that there is no clear way to connect the SRS with the effective value in the measurement location, i.e. it is not possible to distinguish which sources would produce a value in the measurement point that is below the MDC but different from zero.

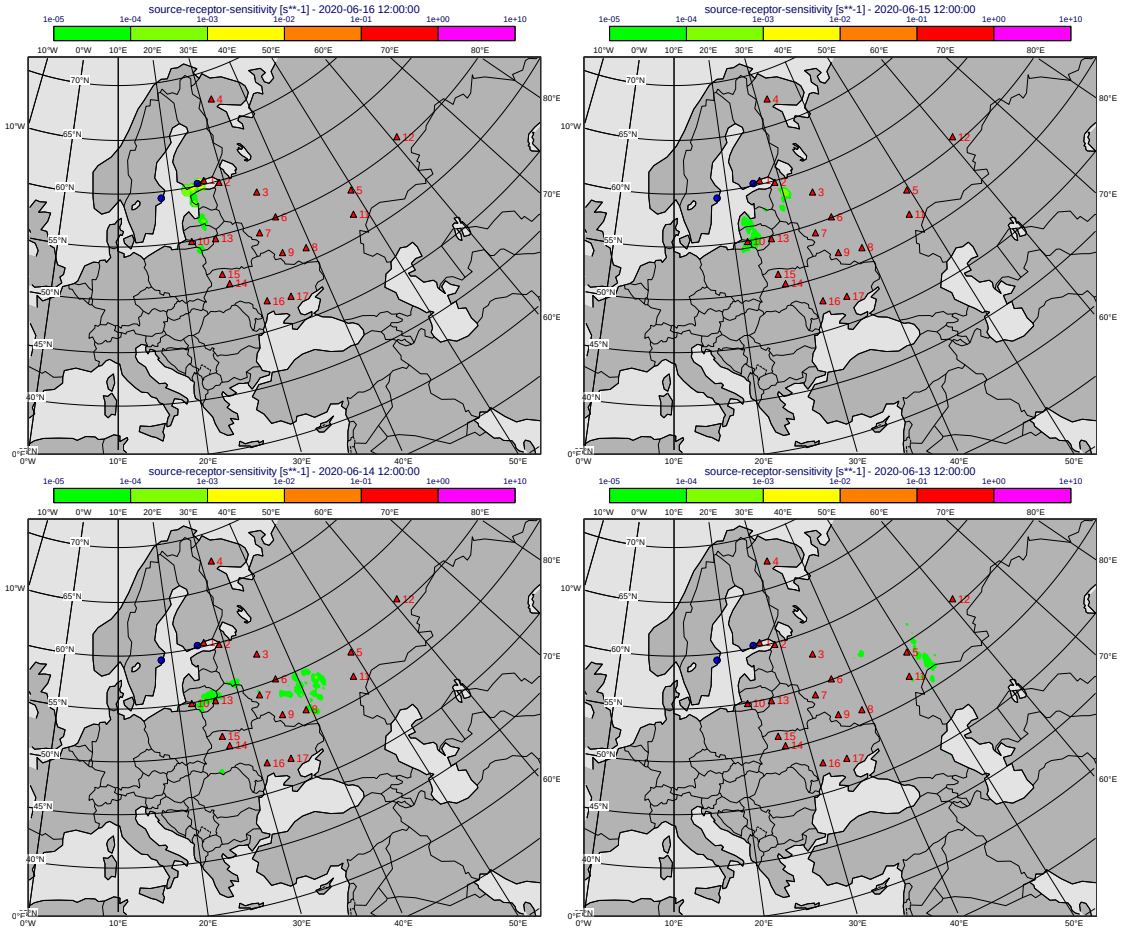

Figure 4.10: Combined backward concentrations for the measurements in Helsinki and Stockholm.

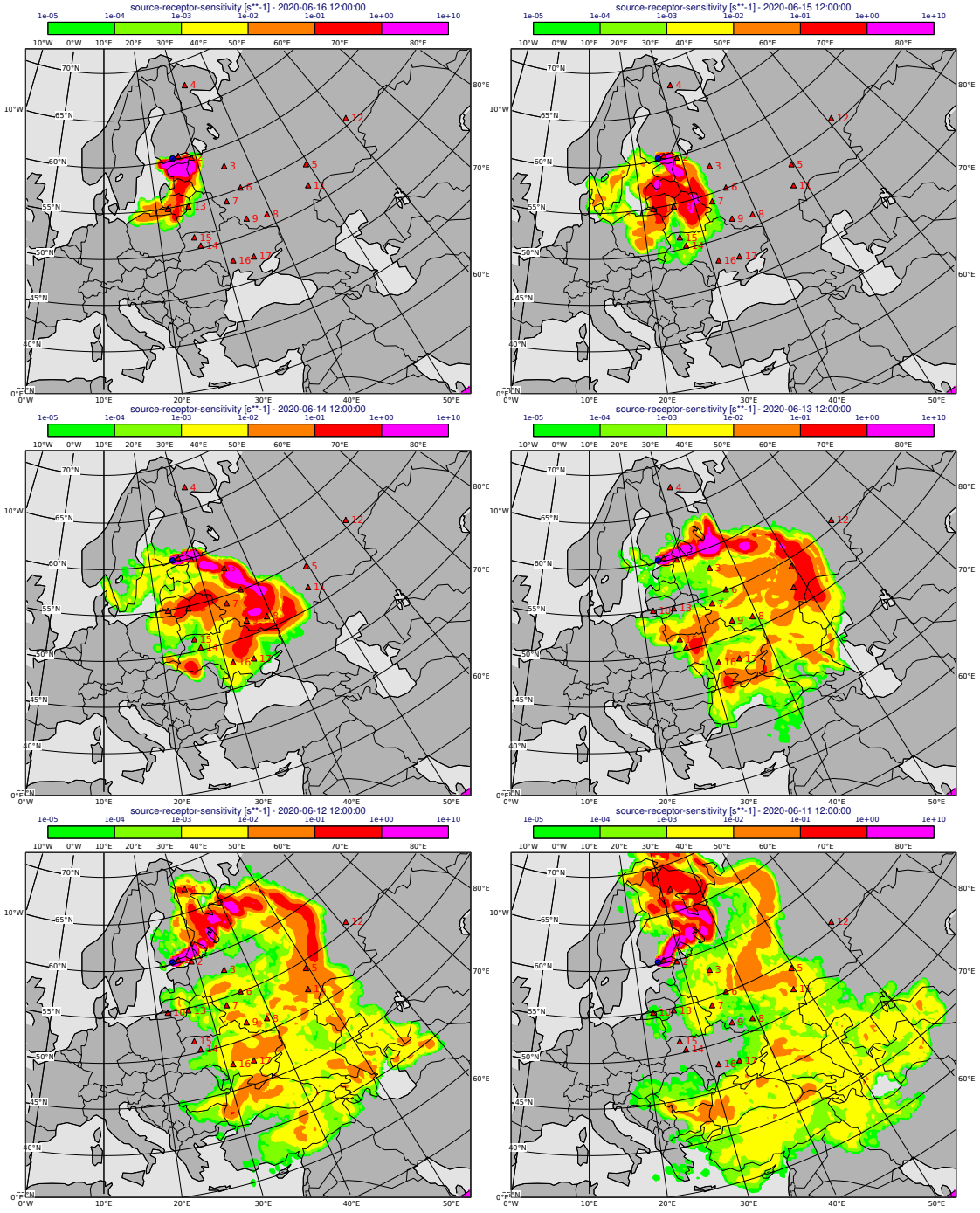

Figure 4.11: Backward concentrations for Helsinki days without a measurement above MDC.

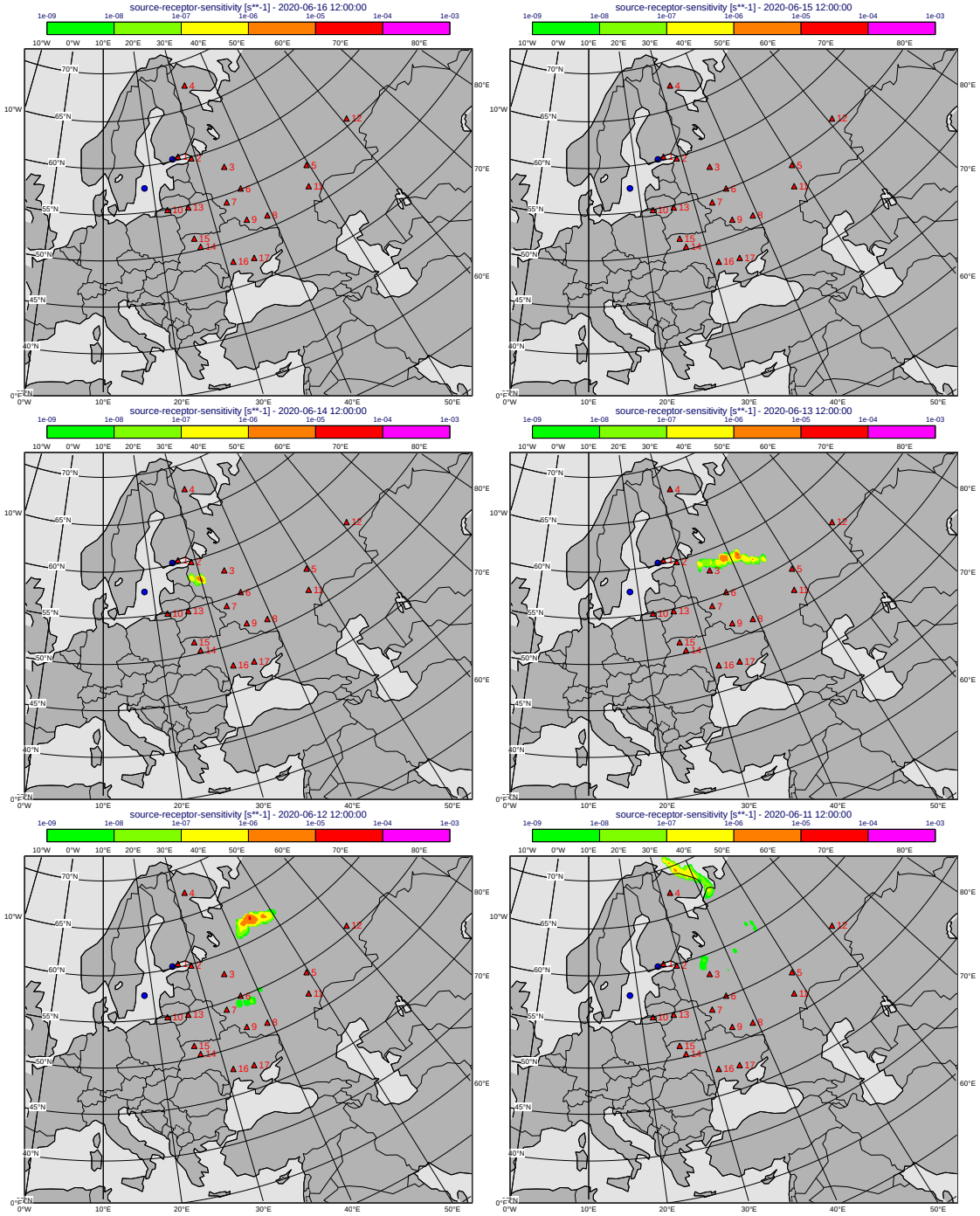

Figure 4.12: Combined backward concentrations for the measurements in Helsinki and Visby taking into account for the missing measurements in Helsinki and Stockholm.

Nevertheless, when combining this simulation with the single simulations from Helsinki and Visby, it is possible to narrow the SRS cloud spread. The result, when selecting a cutoff value for the below-MDC values at $1 \times 10^{-2}\,\mathrm{s}^{-1}$, is shown in Figure 4.12. We can see that the cloud is indeed much narrower with this approach. However, the region affected by the simulation is still quite spread across Eastern Europe without a clearer indication of the possible source.

Figure 4.13 shows how these below-MDC simulations can affect the extrapolated results at the selected nuclear sites varying the cut-off value. As the cut-off becomes lower, more and more points (in space and time) are removed from the graph due to the integration of this latest information. It is, however, difficult to select a cut-off value that is correlated in any significant way to the MDC specific of each measurement station.

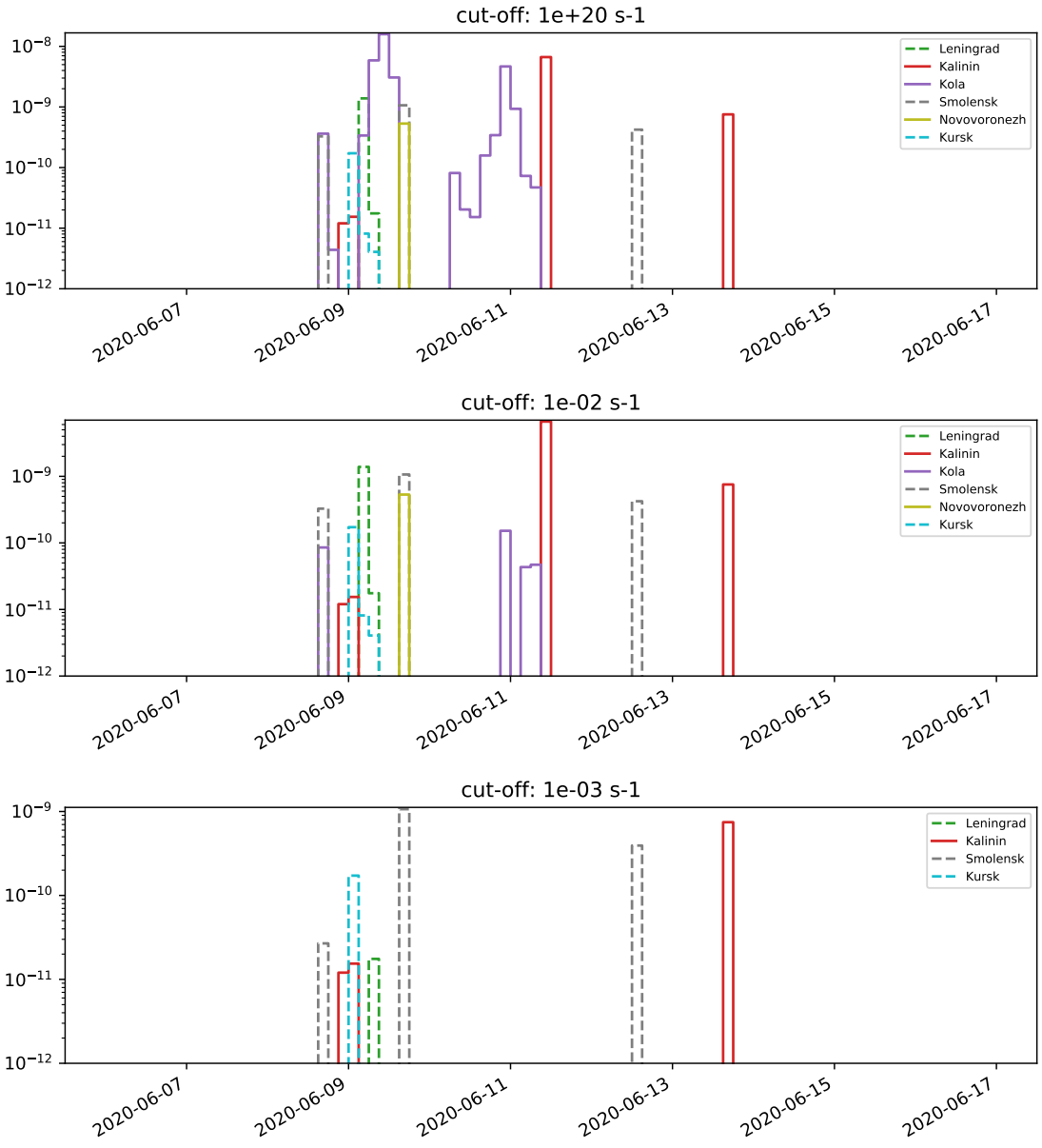

Figure 4.13: Effect of the value of the cut-off for the below-MDC simulations.

5 Conclusions

This report analyzed some anomalous measurements reported from Northern and Eastern Europe during the month of June 2020 exploring some methodologies that can be usefully applied to the determination of the origin of these measurements.

Different and synergic approaches have been employed to possibly pin-point a specific typology, location and time frame of the release that generated the measurements.

First of all, activity concentration ratios of sensible isotopes can be exploited to identify the age of the fuel and the reactor type that could have produced it. Unfortunately, the available data are not in agreement: while the Ru-103 and Ru-106 ratio indicates that at least 80 days must have passed since the reactor shutdown, the ratio between Zr-95 and Ce-141 tells that the reactor shutdown can be at most 25 days in the past. There is only a single available measurement for each of the couples listed, and each of them is for a value that is not far away from the minimal detectable concentration, so it can be affected by sensitivity errors.

For what concerns the Cs-134 and Cs-137, the number of available measurements is far larger. We have already remarked that the ratios do not agree with each other, with values that can vary from 0.6 up to 1.4. Even taking into account for a possible respuspension background from old Cs-137, it is difficult to converge on a coherent value. The most probable scenario involves a VVER-type reactor and fuel extracted after 3 (maybe 2) cycles. Scenarios that involve fuel coming from an RBMK-1000 reactor are far less likely.

All the measurements have been provided with an uncertainty level that corresponds to one standard deviation away from the mean value. This uncertainty seems to be not enough to reconcile the various ratios and build a framework that explains all the values without some heavy assumptions on e.g. the Cs-137 resuspension.

Atmospheric modeling of pollutant dispersion is a powerful tool that can identify possible source locations and timeline of the release. The study of backward trajectories of air masses is a first step that can quickly identify the possible emission regions at a very low computational cost. This analysis has been done for the most relevant measurements, i.e. the ones from Helsinki, Visby and Stockholm. The other measurements, in Kotka and Harku, do not provide additional information since their location is very close to Helsinki and the assimilation period is longer then the Helsinki one.

All trajectories point towards east/south-east, highlighting western Russia and adjoining countries as possible sources. The region includes many nuclear sites, including VVER and RBMK reactors, together with research sites and reprocessing facilities.

Another approach to the backward simulation of the inverse dispersion of a pollutant in the atmosphere is to look at source-receptor-sensitivity matrices generated with backward concentration computations. While quite more expensive than trajectory compu-

tations, concentration simulation can be more useful since they include the contribution of the turbulence in the atmosphere. Another strong aspect of this approach is the possibility to combine multiple sensitivity matrices to obtain a sort of *conditioned probability* that is directly connected to the probability that a certain location is *simultaneously* a suitable source for many different measurements. In this framework it is also possible to integrate the *absence* of a measurement as an additional information in the estimation of the plausibility of a given location.

This kind of approach works best when the measurements are close in time but far away in space. This is not, however, the case here, where all relevant measurements come from Scandinavia and they are subject to a similar atmospheric condition. Furthermore, the Stockholm measurement is quite later in time and therefore its integration with the other data has a minimal impact.

The concentration and trajectory simulations, performed with different codes and different meteorological data, give consistent results that testimony the robustness of the approach that has been followed. The backward concentration simulation offer also more detailed information that can be interpolated to specific locations of interest, but in this situation are not capable of identifying the source location with a sufficient degree of confidence.

Overall, the level of information available for this case study is very limited, mostly due to the very low concentrations of the measured radioactive pollutants. Further information, possibly from different kind of analysis, that would improve the knowledge on e.g. the accuracy of the measurements, the resuspension of Cs-137 in that specific days or the time of the release could be usefully exploited to improve the current results.

Acknowledgements

The authors kindly acknowledge

- the Weather Service of Aeronautica Militare Italiana, for making available to ENEA the ECMWF forecast weather data.
- ECMWF's computing and archive facilities that have been exploited in this research.
- Copernicus Climate Change and Atmosphere Monitoring Services (CAMS) for providing meteorological data that have been used in this research.
- the NOAA Air Resources Laboratory (ARL) for the provision of the HYSPLIT transport and dispersion model and READY website (`https://www.ready.noaa.gov`) used in this publication.

Bibliography

[1] *Ruthenium and Cesium detections in air in Europe*. Tech. rep. IAEA Incident and Emergency Centre, 2020–07–02.

[2] *Technical Attachment Status of Ruthenium and Cesium detections in air in Europe*. Tech. rep. IAEA Incident and Emergency Centre, 2020–07–02.

[3] L. L. Humphries et al. *MELCOR computer code manuals version 2.2.9541*. Tech. rep. 2007.

[4] M. De Cort et al. *Atlas of Caesium Deposition on Europe after the Chernobyl Accident*. Tech. rep. European Commission, 1998.

[5] T. Hopp et al. "Non-natural ruthenium isotope ratios of the undeclared 2017 atmospheric release consistent with civilian nuclear activities". In: *Nature Communications* 11.1 (2020), pp. 1–7.

[6] W. A. Wieselquist, R. A. Lefebvre, and M. A. Jessee. *Scale Code System version 6.2.4*. Tech. rep. ORNL/TM-2005/39, April 2020.

[7] A. Stein et al. "NOAA's HYSPLIT atmospheric transport and dispersion modeling system". In: *Bulletin of the American Meteorological Society* 96.12 (2015), pp. 2059–2077.

[8] G. Rolph, A. Stein, and B. Stunder. "Real-time environmental applications and display system: READY". In: *Environmental Modelling & Software* 95 (2017), pp. 210–228.

[9] A. Cervone, A. Guglielmelli, and F. Rocchi. "Forward and backward analysis of the 2017 release of Ru-106 over Europe using a Lagrangian dispersion model and monitoring station data". In: *EUROSAFE 2019*. GRS. 2019, pp. 279–290.

[10] A. Stohl et al. *The Lagrangian particle dispersion model FLEXPART version 9.3*. Tech. rep. Tech. rep., Norwegian Institute of Air Research (NILU), Kjeller, Norway, 2010.

[11] A. Stohl, M. Hittenberger, and G. Wotawa. "Validation of the Lagrangian particle dispersion model FLEXPART against large-scale tracer experiment data". In: *Atmospheric Environment* 32.24 (1998), pp. 4245–4264.

[12] A. Stohl and D. J. Thomson. "A density correction for Lagrangian particle dispersion models". In: *Boundary-Layer Meteorology* 90.1 (1999), pp. 155–167.

[13] A. Stohl et al. "The Lagrangian particle dispersion model FLEXPART version 6.2". In: *Atmospheric Chemistry and Physics* 5.9 (2005), pp. 2461–2474.

[14] I. Pisso et al. “The Lagrangian particle dispersion model FLEXPART version 10.3”. In: *Geosci. Model Dev. Discuss* (2019), in review.

[15] P. Seibert and A. Frank. “Source-receptor matrix calculation with a Lagrangian particle dispersion model in backward mode”. In: *Atmospheric Chemistry and Physics* 4.1 (2004), pp. 51–63.